Biomaterials Advances 158 (2024) 213765

Contents lists available at ScienceDirect

Biomaterials Advances

journal homepage: www.journals.elsevier.com/materials-science-and-engineering-c

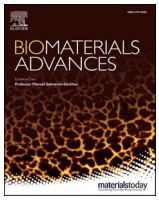

Co-delivery of VEGF and amoxicillin using LP-coated co-axial electrospun fibres for the potential treatment of diabetic wounds

Robyn A. Macartney [a,b,*], Edward Weaver [b], Robyn Irwin [b], Matthew P. Wylie [b], George A. Burke [a], Dimitrios A. Lamprou [b,*]

[a] Nanotechnology & Integrated Bioengineering Centre (NIBEC), School of Engineering, Ulster University, York Street, Belfast BT15 1ED, UK
[b] School of Pharmacy, Queen's University Belfast, 97 Lisburn Road, Belfast BT9 7BL, UK

ARTICLE INFO

Keywords:
Wound healing
Electrospinning
Coaxial fibre
Drug delivery
Microfluidics
Liposome

ABSTRACT

Diabetic complications present throughout a wide range of body tissues, however one of the most widely recognised complications remains to be chronic diabetic wounds. Current treatment options largely rely on standard wound treatment routines which provide no promotion of wound healing mechanisms at different physiological stages of repair. Recently materials produced using novel additive manufacturing techniques have been receiving attention for applications in wound care and tissue repair. Additive manufacturing techniques have recently been used in the interest of targeted drug delivery and production of novel materials resembling characteristics of native tissues. The potential to exploit these highly tailorable manufacturing techniques for the design of novel wound care remedies is highly desirable.

In the present study two additive manufacturing techniques are combined to produce a scaffold for the treatment of diabetic wounds. The combination of microfluidic manufacturing of an antimicrobial liposome (LP) formulation and a coaxial electrospinning method incorporating both antimicrobial and proangiogenic factors allowed dual delivery of therapeutics to target both infection and lack of vascularisation at wound sites. The coaxial fibres comprised of a polyvinyl alcohol (PVA) core containing vascular endothelial growth factor (VEGF) and a poly (L-lactide-co-ε-caprolactone) (PLCL) shell blended with amoxicillin (Amox). Additionally, a liposomal formulation was produced to incorporate Amox and adhered to the surface of fibres loaded with Amox and VEGF. The liposomal loading provided the potential to deliver a much higher, more clinically relevant dose of Amox without detrimentally changing the mechanical properties of the material. The growth factor release was sustained up to 7-days *in vitro*. The therapeutic effect of the antibiotic loading was analysed using a disk diffusion method with a significant increase in zone diameter following LP adhesion, proving the full scaffold system had improved efficacy against both Gram-positive and Gram-negative strains. Additionally, the dual-loaded scaffolds show enhanced potential for supporting vascular growth *in vitro,* as demonstrated *via* a viability assay and tubule formation studies. Results showed a significant increase in the average total number of tubes from 10 in control samples to 77 in samples fully-loaded with Amox and VEGF.

1. Introduction

The detrimental damage to microvasculature is a consequence of diabetic physiology as a result of advanced glycation end product accumulation in tissue and surrounding fluids, causing immense problems in relation to wound healing mechanisms. The development of chronic wounds leads to many amputations across the globe [1]. In 2016 Zhang *et al.* reported that worldwide an estimated 6.8 million people underwent major amputations as a result of diabetic wounds [2]. The diverse range of potential complications experienced as a result of diabetes extensively contribute to the need for these amputations. For example, there is a high incidence for the causation of chronic wounds as a direct result of diabetic neuropathy [3].

There are several well-established methods for managing chronic wounds, however, many of these fall short of the requirements necessary for successful wound healing. The most common approach for the treatment of chronic wounds involves a multistep approach consisting of infection control, surgical debridement, regular dressing, off-loading to

* Corresponding authors.
E-mail addresses: Macartney-R4@ulster.ac.uk (R.A. Macartney), D.Lamprou@qub.ac.uk (D.A. Lamprou).

https://doi.org/10.1016/j.bioadv.2024.213765
Received 5 December 2023; Received in revised form 5 January 2024; Accepted 7 January 2024
Available online 14 January 2024

relieve pressure and maintenance of a moist wound bed [4].

Until recently, diabetic wounds have been treated simply with standard or foam dressings which allow for quick absorption of purulent drainage and protective cushioning of the wound. In recent years the application of alginate and hydrogel dressings has become common practice. Yang *et al.* have recently reported their work on antibacterial hydrogel dressings in an attempt to overcome these shortcomings of conventional hydrogels [5].

Recent popularity in the use of additive manufacturing techniques for the production of biomedical products provides the potential to design customised treatments. Commonly used materials for such fabrication techniques include natural and synthetic polymers. The incorporation of therapeutics such as antimicrobial, anti-inflammatory and bioactive agents to these manufactured scaffolds means they can be used for targeted drug delivery. Targeted and controlled drug delivery has become a highly researched area within pharmaceutical fields with claims that this could help ameliorate problems often encountered in relation to patient compliance and rise of antimicrobial resistance (AMR) [6].

Key identified problems in relation to diabetic wound healing include development of infections at the wound site and lack of vascularisation at wound sites causing reduced nutrient delivery to aid with wound healing mechanisms. Addressing infection concerns have also become more difficult due to rising incidences of AMR and an increased occurrence of both polymicrobial and/or biofilm-forming infections in diabetic wounds [7–9].

Scaffold architecture has a major role in supporting vascularisation, with optimisation of factors such as pore size, porosity and pore interconnectivity playing a major role in promotion of tubular infiltration. However, additional efforts can be employed to further promote the process. One of the most commonly observed methods to enhance vascularisation at wound sites is the incorporation of growth factors to scaffold materials. The ability to incorporate growth factors into polymer scaffolds and directly deliver these to the injury site enhances the potential for tissue repair through normal wound healing mechanisms. VEGF is a growth factor which plays a role in angiogenesis and wound repair. During angiogenesis VEGF promotes endothelial cell proliferation and survival. It has been shown to enhance endothelial cell migration and invasion *via* increasing permeability of existing vessels overall forming a lattice network to facilitate migration [10]. VEGF levels can influence the rate of wound closure and re-epithelialisation and promote granulation tissue formation to provide strength to the healed wound [11].

A key emerging technology in the field of controlled and prolonged API delivery is electrospinning. Electrospun fibres have gained widespread recognition in both drug delivery and tissue engineering fields due to their remarkably customisable characteristics allowing for controlled and prolonged drug delivery rendering them an appealing material for both acute and chronic wound dressings. These dressings could be capable of incorporating and releasing a variety of customised therapeutic agents including both antibiotics and vascularising growth factors [12]. Co-axial electrospinning provides the potential to create highly fibrous scaffolds with a core-shell fibre structure, enabling the sustained or co-delivery of APIs and often enhance other material characteristics such as mechanical and biocompatibility properties [13,14].

A limitation to the sole-use of fibrous scaffolds for time-limited drug delivery systems (DDSs), such as wound dressings, is the capacity to provide a bolus dose of API. The bolus dose may be required to achieve therapeutic levels, especially for disease states such as bacterial infections. To combat this issue, additional dosage *via* nanoparticles is proposed and investigated as a solution throughout this article.

Several different types of nanoparticles have been used for antimicrobial purposes. The formulation of organic nanoparticles using lipid or polymer-based formulations, such as LPs, is a potent means of antimicrobial therapy. LPs are a type of lipid-based nanosystem composed of a concentric bilayer of biocompatible and biodegradable materials. These systems allow the incorporation of drugs, antibodies, proteins or enzymes to provide specific delivery to infection sites [15,16]. Liposomal formulations offer a number of advantages compared to other delivery systems such as the ability to incorporate hydrophilic and hydrophobic drugs, biocompatibility, biodegradability, low toxicity and immunogenicity [17,18]. The incorporation of LPs into electrospun fibres has been frequently reported to improve drug release characteristics [19–21]. However, following liposomal incorporation fibre morphology is often altered, appearing beaded [22–24]. Observation of beading in past studies has been reported to cause knock-on effects on the mechanical properties of the final scaffold [25]. Few attempts have been reported in the literature to graft LPs to the surface of electrospun fibres. One group report a simple method to achieve this liposomal grafting while another reports a method of fibre surface modification *via* thiolation prior to liposomal attachment [26,27]. We propose that by grafting LPs rather than incorporating them into the fibre structure the alterations in the mechanical properties can be avoided.

In this manuscript we report the development of a coaxial electrospinning method enabling the dual delivery of angiogenic growth factor, VEGF, and a model broad-spectrum antimicrobial agent, Amox, to enhance vascularisation potential and prevent infections at wound sites. A water-soluble polymer, PVA, is used as the core layer to incorporate VEGF and facilitate a sustained and controlled release of the angiogenic factor. The outer shell is composed of PLCL, a blend polymer of polycaprolactone (PCL) and poly-L-lactic acid (PLLA), a less readily degradable polymer providing longer term support for wound protection during closure. Within this layer Amox is incorporated to prevent infections at the wound site. As an additional and immediate antimicrobial measure LPs containing Amox are adhered to the fibre surface to provide an immediate burst release of the drug at the time of application. To the authors knowledge this is the first report of a triple layered drug delivery system (DDS) of this type, combining electrospinning and microfluidics, two manufacturing techniques of great interest within pharmaceutical and tissue engineering fields.

2. Materials and methods

2.1. Materials

Poly(L-lactide-*co*-ε-caprolactone) (PLCL) was obtained from Corbion N.*V*. (Amsterdam, Netherlands). Chloroform, dimethylformamide (DMF) and methanol (HPLC grade) were obtained from ROMIL Ltd. (Cambridge, UK). Poly (vinyl alcohol) (PVA), Triton X-100, paraformaldehyde (PFA), hexamethyldisilane (HMDS, cell culture grade), sodium dodecyl sulphate (SDS), 3-(4,5-dimethylthiazol-2-yl)-2,5-diphenyl tetrazolium bromide (MTT), cetylpyridinium chloride (CPC) 1,2-Distearoyl-sn-glycero-3-phosphocholine (DSPC), phosphate buffered saline (PBS) tablets, rhodamine, ethanol (<99 %), sodium phosphate monobasic ($NaH_2PO_4{\cdot}2H_2O$), sodium phosphate dibasic ($NaH_2PO_4{\cdot}7H_2O$) and hexamethyldisilane (HMDS) were all obtained from Sigma-Aldrich (Missouri, US). N-(carbonyl-methoxypolyethylene glycol-2000)-1,2-distearoyl-sn-glycero-3-phosphoethanolamine, sodium salt (DSPE-PEG2K) was obtained from Lipoid (Ludwigshafen Germany). Amoxicillin (Amox) and cholesterol were purchased from Tokyo Chemical Industry (Tokyo, Japan). Cell culture reagents Dulbecco's Modified Eagle's Medium/Nutrient Mixture F-12 Ham (DMEM/F12), Penicillin/Streptomycin, Large Vessel Endothelial Supplement (LVES), foetal bovine serum (FBS), Trypsin-EDTA and the human VEGF-165 recombinant protein were obtained from Thermo-Fisher Scientific (Massachusetts, US). The DuoSet ELISA and ancillary kit were obtained from R&D Systems (Minnesota, US). Human umbilical vein endothelial cells (HUVEC) pooled primary cells were purchased from PromoCell (Heidelberg, Germany). Fluorescent stain DAPI, primary and secondary antibodies were purchased from Invitrogen (Massachusetts, US). *Staphylococcus aureus* (*S. aureus*, ATCC 29213) and *Proteus mirabilis*

(*P. mirabilis*, ATCC 51286) were purchased from ATCC (Virginia, US) and stored on cryopreservative beads at −80 °C. Mueller-Hinton broth was obtained from Oxoid Ltd. (Basingstoke, UK). Any materials where the purity is not stated are EP grade or above.

2.2. Preparation of electrospun scaffolds

Co-axial Electrospun scaffolds were produced using a commercial co-axial nozzle set up (Bioinica, Spain), the composition of fibres was a sheath layer of PLCL and a core of PVA. The PLCL electrospinning solution was 10 wt% PLCL in a solvent solution composed of a ratio of 8:2 (chloroform: DMF). This electrospinning solution was mixed overnight to ensure complete solubilisation of the polymer. The PVA electrospinning solution was also composed of 10 wt% of the polymer in a solvent system of 9:1 (dH_2O:EtOH). This solution was heated to 80 °C for 1 h in a water bath to solubilise the polymer.

For the fabrication of dual-loaded scaffolds, Amox was first dissolved in DMF to a final concentration of 1 % (*w*/w in relation to polymer concentration). Chloroform and PLCL were then added in the same quantities as previously described to form the Amox loaded electrospinning solution. In the PVA solution for dual-loaded scaffolds the polymer solution was allowed to cool, and VEGF was added to a final concentration of 0.1 μg/mL.

Electrospinning parameters were optimized, and final scaffolds were produced using the following equipment parameters. The needle of the injector was connected to a positive electrode, while a rotating mandrel collector was grounded. The inner needle had a diameter of 22 G while the outer needle had a diameter of 15 G. A high voltage of 20 kV was applied to the needle tip, at 20 cm from the collector. The flow rate of the PVA and PLCL solutions were set to 0.2 mL/h and 1.2 mL/h respectively. Scaffolds were spun until 2 mL of PLCL had been dispensed to allow adequate scaffold thickness for following studies.

2.3. Preparation of amox-loaded LPs

LPs were fabricated using a microfluidics technique, an aqueous and lipid phase were used with the Amox incorporated into the aqueous phase for encapsulation into a self-assembling lipid bilayer. LPs were formulated using three reagents, DSPC, DSPE-PEG2K and cholesterol to a total lipid concentration of 1 mg/mL with a 1:1:1 ratio of each reagent. For initial adhesion studies a second formulation consisting of only DSPC, and cholesterol was used, again with a total lipid concentration of 1 mg/mL and a 2:1 mass ratio of DSPC: cholesterol. In both cases the aqueous phase including the antimicrobial agent was a 1 mg/mL Amox solution in PBS. The LPs were produced using an in-house 3D-printed microfluidic chip, as previously reported [28], at a flow rate ratio (FRR) of 5:1 (aqueous: lipid) with a total flow rate (TFR) of 6 mL/min. Excess ethanol was subsequently removed *via* evaporation using a hot plate and stirrer for 30 min at 37 °C.

2.4. Liposomal adhesion to fibre surface

For the LP adhered scaffolds, following spinning of drug loaded co-axial scaffolds they were immersed in a liposomal solution in a ratio of 1 mL per cm^2 of scaffold. These were placed on an orbital shaker for 2 h at room temperature to facilitate liposomal adhesion. After adhesion, samples were gently washed three times in deionised water and dried in a desiccator overnight before use in further experiments.

2.5. Scaffold characterisation

2.5.1. Scanning electron microscopy

All images were collected in secondary electron mode using an accelerating voltage of 5 kV, at a working distance of 5 mm and at magnifications between x90 and x20000. Using Image-J with Diameter-J plug in, physical characteristics of the materials such as fibre diameter were quantified.

For SEM imaging of LP adhered samples and during cell studies samples were subjected to several processing steps prior to imaging. Samples were first fixed using Karnovsky's fixative (4 % PFA, in a 0.2 M sodium phosphate buffer, pH adjusted to 7.4 using HCL/NaOH), washed three times in DI water to remove traces of fixative before being subjected to an alcohol dehydration series of increasing EtOH concentration between 25 % and 100 %. *v*/v. Finally, samples were chemically dried overnight using hexamethyldisilane (HMDS). All samples for SEM imaging were deposited with a thin layer conductive coating (~13 nm) using an Emitech K500X sputtering system (Quorum Technologies, UK) fitted with a gold-palladium target at 25 mA for 2 min.

2.5.2. Fluorescent imaging of adhered LPs

To fluorescently label LPs for imaging rhodamine was added to the aqueous phase during manufacturing. The LPs were then adhered to scaffold surfaces as previously described (Section 2.4), dried, and mounted for fluorescent imaging. Images were taken using an upright AxioImager fluorescent microscope (Zeiss, Germany) at excitation: emission of 556:573 nm and magnification of x40.

2.5.3. Raman spectroscopy

Chemical characterisation was carried out *via* vibrational spectroscopy using an, inVia™ confocal Raman microscope, (Renishaw, UK). Raman spectra were obtained of pristine co-axial electrospun PLCL/PVA, dual-loaded scaffolds and those with LPs adhered. Raman parameters were optimized as follows; 785 nm wavelength laser at 50 % power (25 mW) over an extended scan wavenumber range of 100–3200 cm^{-1} with 10 s exposure time using a x50 objective lens. Spectra were subjected to two data processing steps, (i) baseline subtraction and (ii) normalisation by Raman intensity range using '1' as the upper range and '0' as the lower range. Spectra for each material were obtained in triplicate with the spectra presented here representing an average of the 3.

2.5.4. Mechanical analysis

A tensile testing method was established to assess the mechanical properties of the scaffolds produced. Using the testing method, properties such as, ultimate tensile strength, maximum strain to failure and Youngs' modulus were calculated. Samples were cut to dog-bones of the following original dimensions, gauge length 20 mm, cross sectional area 0.04 mm^2 and thickness 0.02 mm following guidelines detailed in ASTM-D882 for the testing of tensile properties of thin plastic/polymer sheeting. For analysis of LP adhered scaffolds, the dog bone samples were cut prior to LP adhesion to prevent any liposomal damage during sample preparation. Testing was carried out on an Instron 5660 series machine (Instron, USA) fitted with a 50 N load cell. Pneumatic grips were used to secure the sample in the apparatus. A crosshead speed of 10 mm/min was used, with measurements collected at a rate of 10 data points per second. Data was converted to stress and strain and plotted as a stress strain curve. Youngs' modulus values were calculated from the initial linear elastic region of the curve. Results reported represent an average of 5 repeat samples.

2.6. Total LP loading and in vitro drug release

To determine the maximum Amox loading of the scaffolds with LPs adhered a scaffold was placed in dialysis tubing with 1 mL of chloroform to fully dissolve the sample. This was then dialysed against 4 mL of fresh PBS using the cellulose dialysis tubing with molecular weight cut-off of 14 kDa for 2 h at room temperature. A 0.5 mL aliquot of release media was collected, and the following high performance liquid chromatography (HPLC) method was used to quantify the total Amox content of scaffolds. The test was completed in triplicate and the average of the three samples was used as the maximum release for calculating percentage cumulative release.

For Amox release from the dual-loaded scaffolds, samples of 4 cm^2

were placed in dialysis tubing (cellulose tubing, MWCO 14 kDa) with 1 mL of PBS and submerged in 4 mL of PBS at 37 °C. Aliquots of 0.5 mL release media were removed at 0.5, 1, 2, 4, 5, 6, 24, 48, 72, 96, 120, 144, 168 and 192 h and replaced with fresh pre-warmed PBS.

UV-HPLC was used to quantify Amox content and release from the drug loaded scaffolds. Here the analysis was carried out using a reverse phase C18 column (250 mm × 4.6 mm, ThermoFisher, US) with UV-detection wavelength of 278 nm at ambient temperature, using an injection volume of 50 μL. The mobile phase used was composed of a sodium dihydrogen monohydrate buffer (adjusted to a pH of 5 ± 0.05 using ortho-phosphoric acid), mixed with HPLC grade methanol in a ratio of 95:5 (*v*/v). A flow rate of 1 mL/min was used for the duration of the experiment and the run time for each sample was set to 15 mins.

VEGF release was quantified using a human VEGF ELISA kit obtained from R&D Systems (Minnesota, US). Scaffolds were cut to a cross sectional area of 25 cm^2 and immersed in 15 mL of PBS with 1 mL sample aliquots removed and replaced with fresh PBS at set timepoints. The kit was used as recommended by the manufacturer in combination with the ancillary kit (R&D Systems, US). Briefly, ELISA plates were prepared by coating with the capture antibody (1 μg/mL) overnight at room temperature, washing in wash buffer (0.05 % *v*/v Tween 20 in PBS) and blocking using 1 % *w/v* bovine serum albumin in PBS. To perform the assay, standards and samples were aliquoted in triplicate incubated at room temperature and washed using the wash buffer before addition of streptavidin-HRP. Samples were washed and incubated in substrate solution at room temperature then the reaction was terminated using the stop solution. Samples were read at 405 nm using a Tecan Spark microplate reader (Tecan, Switzerland).

Calculation of cumulative release in mg/mL and percent was conducted using Eqs. (1) and (2).

$$Total\ Release_{Tx} = \frac{A_x}{G} \times D \tag{1}$$

Eq. (1)) The equation used to calculate total release from scaffolds at time *x*, where A_x = area under the peak at time x, G = gradient of the calibration curve and D = dilution factor.

$$Cumulative\ Release_{Tx}(\%) = \frac{Release_{Tx} + Release_{Tx-1}}{Maximum\ release} \times 100 \tag{2}$$

Eq. (2)) The equation used to calculate cumulative release from scaffolds at time x, where $Release_{Tx}$ = total release at time x, $Release_{Tx-1}$ = total release at time x-1 and Maximum release = full possible release from the scaffold determined either experimentally (Amox) or theoretically (VEGF).

2.7. Antibacterial assessment

An adaptation of the EUCAST disc diffusion method was used to assess the antimicrobial efficacy of the scaffold systems as previously described [29]. Both Gram-positive (*Staphylococcus aureus* (*S. aureus*, ATCC 29213)) and Gram-negative (*Proetus mirabilis* (*P. mirabilis*, ATCC 51286)) bacterial strains were incubated for 18 h in an orbital motion incubator at 37 °C and 100 rpm in Muller-Hinton broth (MHB) to prepare an overnight broth. The broth was then centrifuged at 3000 rpm for 12 min, a small amount of the bacterial pellet was resuspended in fresh MHB, and the concentration was adjusted to 1 × 10^8 cfu/mL using a spectrophotometer to assess turbidity and adjust to optical densities of 0.3 and 0.1 for *S. aureus* and *P. mirabilis* respectively. Sterile cotton swabs were used to inoculate Muller-Hinton agar (MHA) plates, plates were swabbed horizontally from top to bottom. This was repeated twice more with the plate rotated 60° each time to ensure complete coverage of the agar plate. Plates were allowed to air dry for 5 min before placement of disks with an area of 1.9 cm^2 of control (PLCL/PVA), dual-loaded (PLCL-Amox/PVA-VEGF), and dual-loaded + LP (PLCL-Amox/PVA-VEGF + LP) on the surface in the centre of the agar plate and incubated at 37 °C until set time points. At set time points the width of the inhibition zone with no bacterial growth, including the sample width, was measured, and recorded. A total of 5 samples were analysed for each group. The test was carried out for a total of 7-days.

2.8. Cell studies

Pooled primary human umbilical vein endothelial cells (HUVEC) were obtained from Promocell (C-12203) and maintained under normal cell culture conditions (5 % CO_2, 37 °C) in DMEM/F12 media supplemented with LVES growth supplement and 1 % penicillin streptomycin. Cells were passed at 70–80 % confluence using 0.025 % *w/v* trypsin-EDTA, pelletised at 1200 rpm for 5 mins, supernatant discarded to remove spent media and the pellet resuspended in fresh growth media. During experimental studies an additional FBS supplement was added to the growth medium to a final concentration of 10 % *v*/v and all experiments were conducted between passages three and seven.

2.8.1. Cell viability

Cell viability was analysed using 3-(4,5-dimethylthiazol-2-yl)-2,5-diphenyl tetrazolium bromide (MTT). For this study cells were seeded at a density of 1 × 10^5 cells/mL and incubated at 37 °C, 5 % CO_2 for 1, 3 and 7 days with media aspirated and replaced at day 3. At each timepoint, MTT solution (5 mg/mL in PBS, filter sterilised) was added to a final concentration of 0.5 mg/mL and incubated at 37 °C until the formazan crystals could be observed visually. Culture media was removed, and a solubilisation buffer added (20 % *w/v* SDS prepared in a 1:1 ratio of DMF: deionised water, pH adjusted to 4.7 using acetic acid). Samples were briefly agitated in the dark until complete solubilisation of the formazan crystals. Following solubilisation, samples were aliquoted in triplicate in a 96 well plate and absorbance was read at 572 nm using a microplate reader (Tecan, Switzerland).

2.8.2. SEM tubule formation

HUVEC cells were seeded as previously described at a density of 5 × 10^5 cells/mL, and cultured under normal conditions (*n* = 3 per sample group). At the set time points of 6 h and 7 days samples were removed from the incubator and washed gently three times in sterile deionised water. Karnovskys' fixative was then applied for 1 h at room temperature. Again, samples were washed three times before application of an ethanol series of gradually increasing concentration from 25 %–100 % *v*/v to gently dehydrate the cells. Samples were then dried overnight using a HMDS chemical drying agent. Prior to imaging samples were coated using a gold-palladium sputtering system as previously described in Section 2.5.1.

2.8.3. Tubule staining assay

HUVEC cells were seeded as previously described at a density of 5 × 10^5 cells/mL and cultured under normal conditions. For immunocytochemistry analysis samples were removed after 14 days of culture and washed twice in ice cold PBS before fixing using 4 % *w/v* paraformaldehyde. Samples were then permeabilised using 0.1 % Triton-X100. Samples were washed three times in PBS and incubated in the primary antibody (CD31 or Von Willebrand Factor (vWF)) at a concentration of 4 μg/mL in antibody diluent (1 % w/v bovine serum albumin, 5 % *v*/v normal goat serum in PBS) for 60 min at room temperature. Following three washes in PBS the appropriate secondary antibody was added at a concentration of 5 μg/mL (in antibody diluent) for 60 min at room temperature. Nuclei were counterstained using DAPI at a concentration of 600 nM in PBS for 3 min at room temperature. Samples were washed, mounted and covered with a coverslip before imaging using an AxioImager fluorescence microscope (Zeiss, Germany).

Samples stained for vWF allowed observation of the formation of capillary like structures. Image analysis software was to analyse five

images taken at random fields of view and tube formation was analysed according to total tubule length, number of branching points and total number of tubes ($n = 3$ for each group).

2.9. Statistical analysis

Statistical analysis was carried out on data where possible. Mean values are presented as mean ± standard deviation. Statistical significance of appropriate data was tested by one way analysis of variance (ANOVA) and unpaired *t*-test in Prism software (GraphPad Software, Inc., USA). Unless otherwise stated, confidence intervals were set to 95 % and notation used for statistical significance throughout analysis is as follows; * = $P \leq 0.05$, ** = $P \leq 0.01$, *** = $P \leq 0.001$.

3. Results and discussion

3.1. Physical characterisation of scaffolds

Representative SEM images are provided in Fig. 1A–B for both native PLCL/PVA scaffolds and dual-loaded scaffolds. Images demonstrate fibre distribution, morphology, and orientation. There are no visually discernible differences in the physical characteristics between the native and dual-loaded scaffolds, this is confirmed *via* image analysis techniques to calculate the mean fibre diameter obtained for both scaffold groups. Mean fibre diameters of the native and dual-loaded scaffolds are reported as 1.48 ± 0.08 μm and 1.42 ± 0.10 μm respectively. Although mean fibre diameters for the drug loaded scaffolds were calculated as slightly reduced, statistical analysis showed that the difference in fibre diameter after the addition of the Amox and VEGF to electrospinning solutions of PLCL and PVA is negligible. Following the successful fabrication of reproducible scaffolds, a method for adhesion of LPs to the fibre surfaces was investigated. A method described previously by Staffa *et al.* was adapted to achieve successful nanoparticle adhesion and imaging [26]. Initially a liposomal formulation using DSPC was used to encapsulate Amox for adhesion studies. Results from an SEM study, Fig. 2A and D, show that some liposomal adhesion was achieved using this formulation however the quantity of LPs adhered did not appear to be of the same level as that observed previously by other research groups [27]. To enhance the liposomal adhesion a pegylated formulation was produced (DSPE-PEG). It can be seen in Fig. 2B and E that the quantity of LPs adhered was greater than those formulated using the DSPC lipid. It is thought that the pegylated LPs demonstrated enhanced adhesion due to

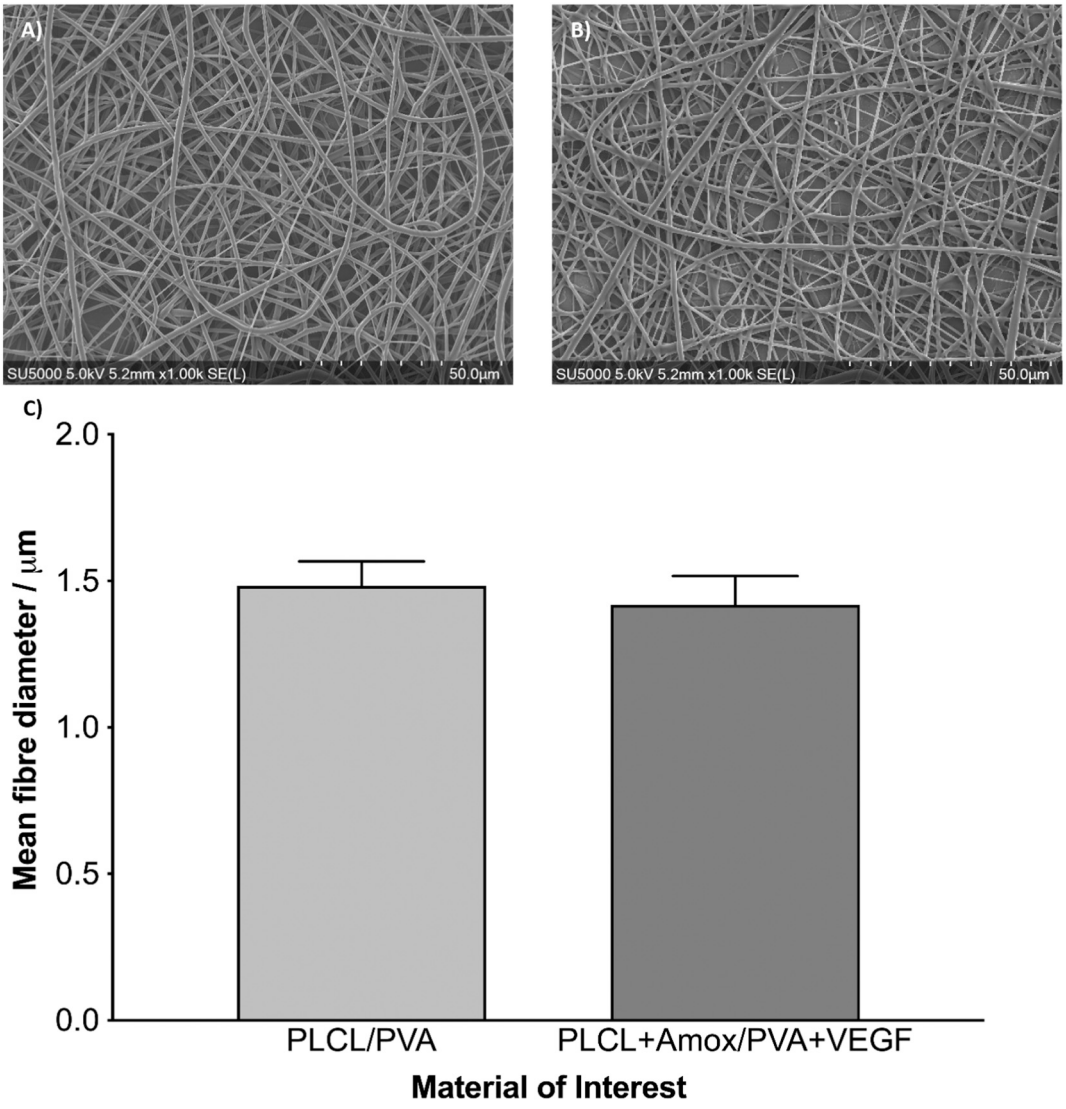

Fig. 1. Physical analysis of scaffolds produced *via* the co-axial electrospinning technique. A–B) SEM images showing the morphology of fibres, A) PLCL/PVA B) PLCL+Amox/PVA + VEGF. C) Calculated average fibre diameters of native and dual loaded coaxial fibres showing no statistically significant change following drug loading.

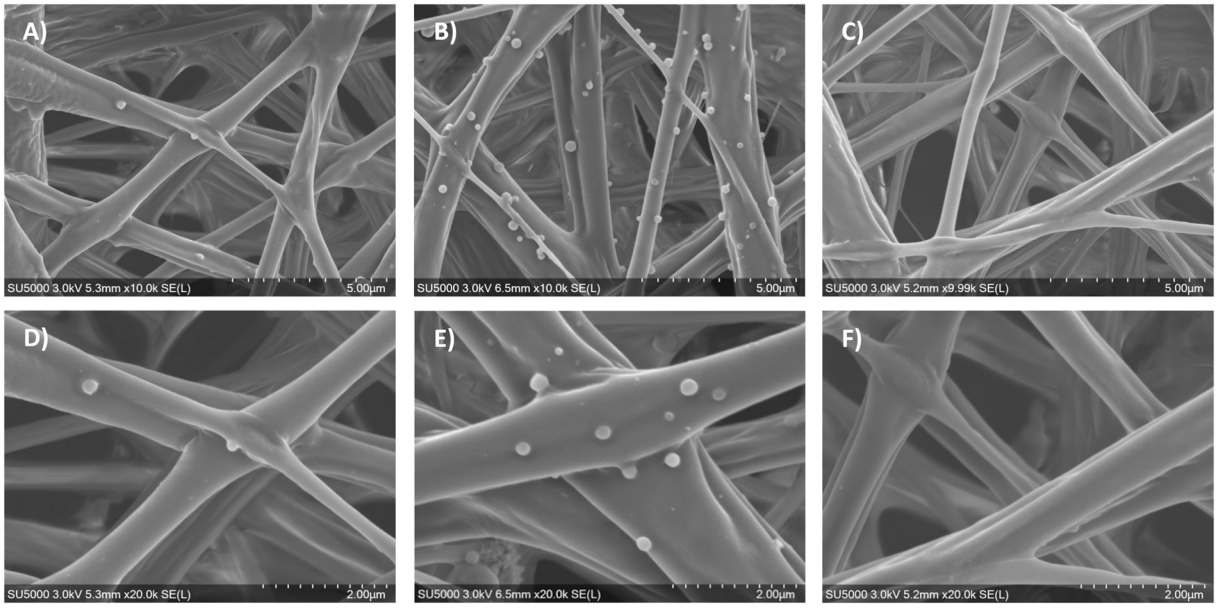

Fig. 2. Representative SEM images showing liposomal adhesion to the co-axial electrospun PVA-Amox/PLCL-VEGF scaffolds at low, ×10,000 (A, C, E) and high ×20,000 (B, D, F) magnification. A & D) DSPC LPs. B & E) DSPE-PEG LPs. C & F) Control co-axial fibres.

the presence of additional long hydrocarbon chains as a result of the pegylation which facilitated increased intermolecular van der Waals attractive forces between LPs and the polymer fibres. Additionally, pegylation is likely to increase hydrogen bonding between terminal hydroxyl and oxygen groups and the PLCL scaffold material. In order to further confirm LP adhesion and assess the uniformity of the liposomal dispersion fluorescent microscopy was used as a qualitative analytical technique. Supplementary information: Fig. 1 shows fluorescent micrographs of samples (A–B) with rhodamine conjugated LPs adhered and (C) without, rhodamine conjugated LPs adhered. A strong fluorescent signal is clearly obtained for both the DSPC and DSPE-PEG adhered samples while there is no signal obtained for the native coaxial fibres, further confirming the successful adhesion of the LPs using this technique. Additionally, the fluorescence image shows that the rhodamine LPs appear evenly distributed across the surface of the coaxial fibres for both the DSPC and DSPE-PEG samples.

3.2. Chemical characterisation of scaffolds

Raman spectroscopy was used to investigate chemical changes to electrospun fibres following dual-loading with VEGF and Amox, and adhesion of LPs. Peaks characteristic of the PLCL and PVA were observed in all the spectra presented in Fig. 3 with bond attributions summarised in Supplementary information: Table 1. No differences were observed in the spectra between the native PLCL/PVA scaffolds and those containing the VEGF and Amox, it is proposed that this is due to the very low concentrations of drug incorporation in comparison to the quantity of polymer in the system. There are however changes to the spectra

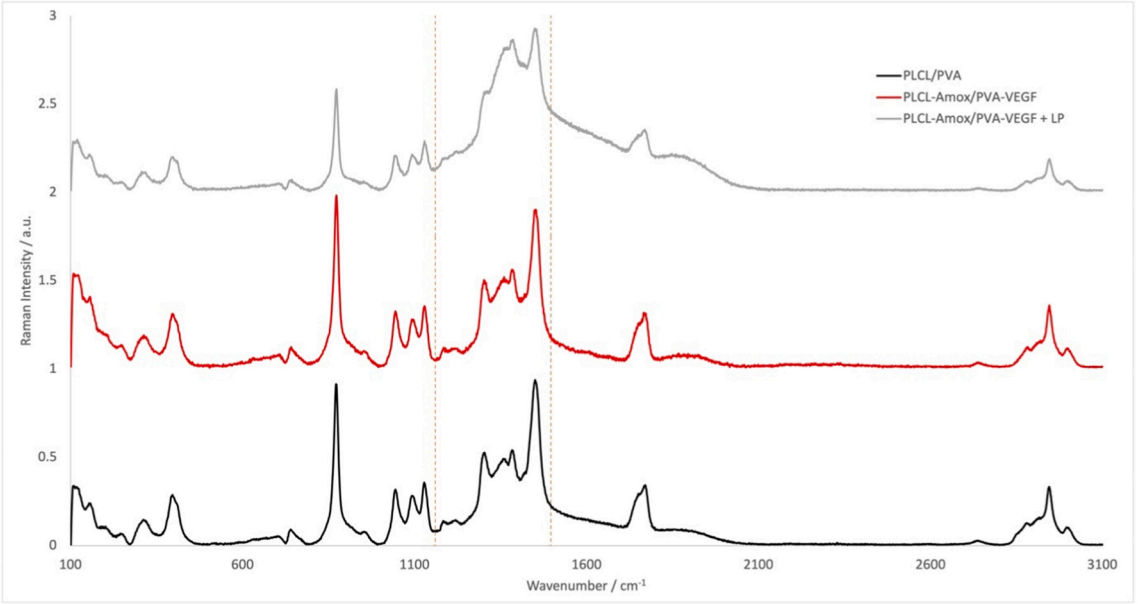

Fig. 3. Raman spectra of native coaxial electrospun scaffolds, dual-loaded electrospun scaffolds and dual-loaded scaffolds with LPs adhered with the region within the dotted lines demonstrating the area of increased Raman intensity following liposomal adhesion.

following liposomal adhesion, whilst no new peaks are observed in the spectra, some increased intensity is observed between 1160 cm^{-1} and 1496 cm^{-1}, as highlighted in Fig. 3. Most characteristic peaks in Raman spectra for lipids are related to the hydrocarbon chains present in all lipids [30]. These peaks are generally observed in three ranges which lie inside the area of increased intensity within the fingerprint region of spectra presented here. Between 1400 and 1500 cm^{-1} the scissoring and twisting deformations of CH_2 are observed, this bond is found within the chemical structure of the polar head of the DSPE-PEG used in the liposomal formulation. The CH_3 scissor and twist deformations are observed between 1250 and 1300 cm^{-1} at an increased intensity in the spectrum obtained following LP adhesion, this bonding is found in the DSPC lipid again within the polar head. Additionally, it is reported that some peaks for bonds present within the chemical structure of Amox can be found within this range which may also contribute to the increased Raman intensity in this range [31].

3.3. Mechanical characterisation of scaffolds

The mechanical properties of scaffolds were analysed using a tensile testing method to ensure suitability of the scaffolds for the intended application. Ideally the mechanical properties should match as closely as possible those of the native tissue intended for repair and replacement. Analysis of the mechanical properties of each scaffold group show that the addition of the Amox and VEGF to the coaxial formulation caused significant changes in the mechanical properties of the scaffolds (Supplementary information: Fig. 2). The ultimate tensile strength was slightly increased along with the Young's modulus; these results suggest that the addition of the therapeutics to the fibres is caused increased stiffness in comparison to the native PLCL/PVA scaffolds. This increase in stiffness corresponds with a reduction in elastic modulus, which given the application of wound dressings may cause problems in terms of failure to meet the native tissue properties for successful treatment. The mechanical properties of drug loaded scaffolds with LPs adhered were also investigated. Interestingly, following liposomal adhesion the scaffolds possessed mechanical properties more closely matched to those of the native PLCL/PVA scaffolds. It is considered that this may be due to the method used for adhesion of LPs to the scaffold surfaces. Here a simple method of submerging samples in a liposomal solution was used, during the time of contact with surrounding liquid it is expected that a degree of fibre swelling will occur. Swelling of polymer networks has been previously described to lead to swelling-induced tensions causing stretching, bending and deformation at both microscopic and macroscopic scales [32]. The effects of solvent uptake on material swelling and induction of mechanical changes has been demonstrated by materials in nature, the human body and synthetic materials [33–35]. Similarly, to the results obtained here, Elhaouzi *et al.* reported a reduction in both Young's modulus and yield stress, for samples following swelling [36]. While it is possible that the presence of the LPs on the fibre surfaces may cause some changes in mechanical properties, evidence in the literature suggests that the changes in mechanical properties following liposomal attachment are at least in part attributed to the adhesion method employed for this study. In respect to the native tissue properties, the skin displays highly anisotropic properties with mechanical properties very much dependent on the location of the tissue, loading rate and age of the skin [37–39]. Additionally, the mechanical test method can greatly influence the mechanical properties displayed making the mechanical characteristics difficult to define, the range of values reported for the Young's modulus of native dermal tissue has been reported to be anywhere within the range of 5 kPa-140 MPa [37]. Ultimate tensile strength (UTS) of native dermal tissue reportedly lies between 0.1 and 40 MPa meaning the scaffolds produced here with UTS of 9.77–13.08 MPa lie well within this range (Table 1) [40–42]. Lack of clarity on the mechanical properties of skin make it difficult to define parameters for the scaffold material. However, based on reports throughout the literature the scaffolds produced in this study possess a suitable elastic modulus for use in wound care applications.

Table 1
Mean values calculated for each of the mechanical properties investigated.

Material	Mean UTS ± SD/MPa	Mean max strain ± SD/%	Mean Young's modulus ± SD/MPa
PLCL/PVA	9.77 ± 1.79	155.57 ± 13.83	37.70 ± 4.89
PLCL + Amox/PVA + VEGF	13.08 ± 1.55	132.47 ± 14.86	55.89 ± 8.47
PLCL + Amox/PVA + VEGF + LPs	11.90 ± 1.84	139.11 ± 5.24	41.87 ± 9.22

3.4. In vitro drug release

3.4.1. Amox release

Fig. 4A–B, shows the release of Amox from the scaffolds. It was observed that both coaxial scaffold groups demonstrated a burst release characteristic of Amox from the PLCL shell layer. This initial release phase lasted for ~5 h in the samples without LPs adhered and 6 h in the LP adhered scaffolds (phase I release). Following the initial burst release, the rate of release subsided but continued in all samples for up to 7 days (phase II release). The data in Fig. 4B shows that during the burst release phase, the LP adhered scaffolds demonstrated a greater percentage cumulative release, this increased percentage release is expected as the LPs themselves demonstrate up to 74 % drug release within the first 4 h of incubation, as reported previously [43]. During the phase II release the percentage drug release in the scaffolds with LPs adhered increased by 13.6 % whereas the scaffolds without LPs adhered increased at an elevated rate of 17.6 % within the same time frame. Taking into consideration the quantity of drug released (Fig. 4A) the inclusion of Amox loaded LPs on the scaffold surfaces significantly enhanced the potential for drug delivery to the wound site with the inclusion of LPs in the delivery system providing a 6.47-fold increase in Amox delivery from 20.95 μg/scaffold to 135.59 μg/scaffold over 7 days. Previous studies using the same bacterial strains used in the current study with solely the liposomal formulation described have shown that the minimum inhibitory concentrations were 6–12 μg/mL and 3 μg/mL respectively for *S. aureus* and *P. mirabilis* respectively (data not shown). Therefore, the levels of release observed for the scaffold systems described here would likely be sufficient to prevent further bacterial growth, due to the high rate of Amox release during the initial 6 h. The results shown in Fig. 4A are encouraging as the level of Amox delivery obtained using the LP coated scaffolds would not be feasible from the electrospun fibres alone as there are several limiting factors concerning the amount of drug which can be loaded without detrimentally effecting the physical and mechanical properties of the scaffolds [44]. At 7 days the total cumulative release from the coaxial PLCL-Amox/PVA-VEGF scaffolds and PLCL-Amox/PVA-VEGF + LP scaffolds was 40.29 % and 45.34 % respectively, it would be expected that any remaining Amox would be released during scaffold degradation as demonstrated throughout the literature [45–47]. Both phases of drug release fitted best the Korsmeyer-Peppas model of drug release, this is unsurprising due to the polymeric composition and cylindrical shape of the fibres both characteristic features leading to this release mechanism [48]. Here R^2 values of 0.99 and 0.97 for phase I and phase II of release respectively, confirm that the data obtained appropriately fits this model (Supplementary information: Table 2). During the data modelling attention was given to the release exponent, values of 0.76 and 0.79 were obtained for stage I release in the coaxial scaffolds and those with LPs adhered respectively. However, during stage II release much lower values of 0.10 for both scaffold groups were recorded for the two scaffold groups. Higher release exponent values suggest that the phase I Amox release is as a result of fibre swelling facilitating anomalous transport diffusion during the initial contact with the release media. The lower release exponents observed during the second release phase suggest a Fick-type

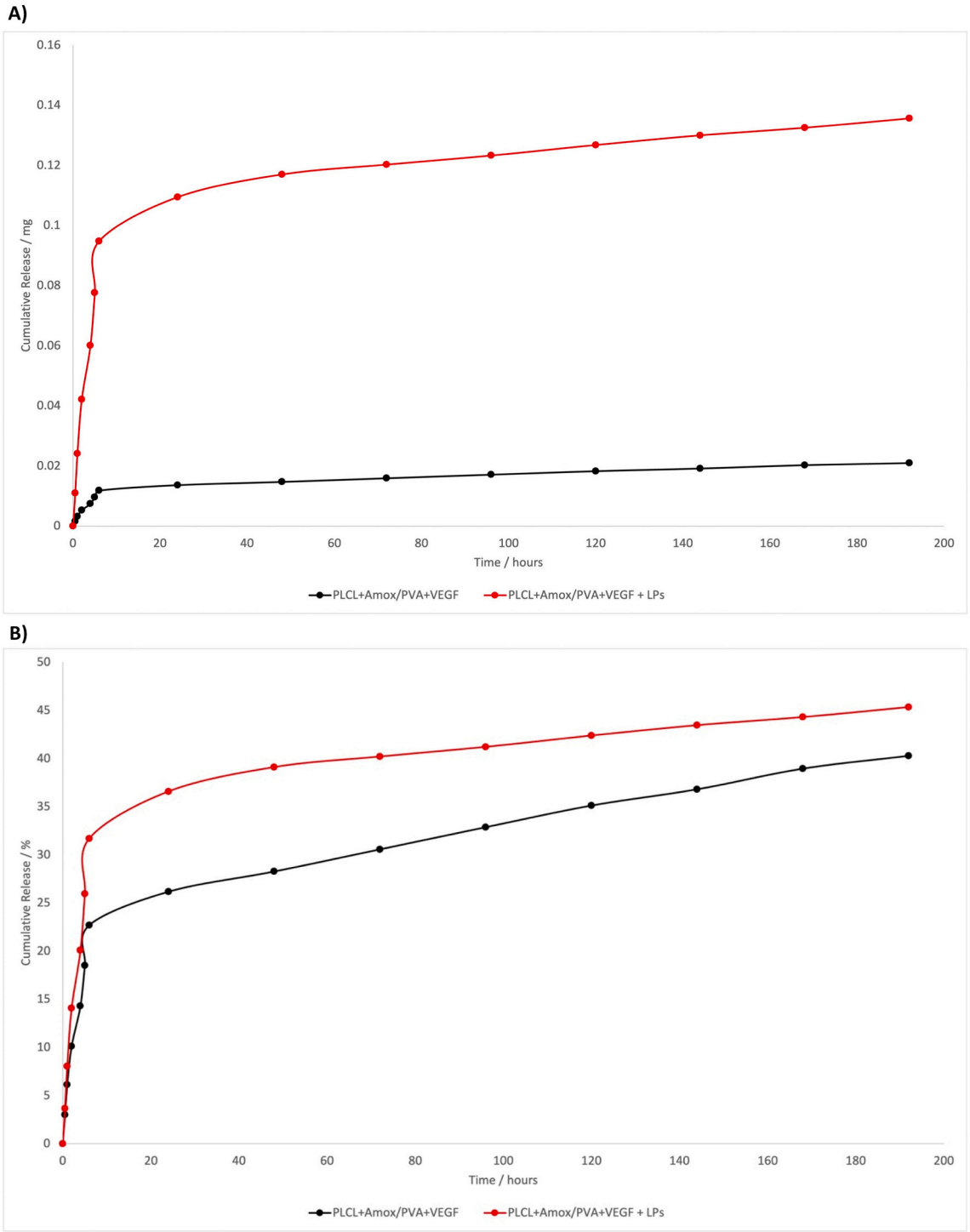

Fig. 4. Cumulative release of Amox from the drug loaded formulations A) quantity release expressed in mg B) release expressed in % as calculated based on values of maximum Amox loading determined experimentally *via* the scaffold destruction technique described.

diffusion of the drug through the fused membrane structure [49,50]. The release of amoxicillin by the scaffolds produced here follows a similar profile to Electrospun scaffolds produced by previous groups to incorporate chloramphenicol and dexamethasone [51,52].

3.4.2. *VEGF release*

The growth factor release was investigated separately using ELISA for the quantification of VEGF release. Fig. 5A–B shows the VEGF release profile for both the dual-loaded coaxial scaffolds and those with LPs adhered. The cumulative release of VEGF demonstrated sustained release for up to 7 days, at which time the total release for coaxial scaffolds was 95.9 % whilst the scaffolds with LPs adhered demonstrated only 66.3 % release. While it is possible that the adhered LPs may alter the release kinetics of the VEGF, it is hypothesised that this reduced percentage release is due to the time of submersion of scaffolds in the liposomal solution during the adhesion process. It is suspected that during this 2-h time period the VEGF release begins. This conclusion seems appropriate as within the first 2 h of the drug release for PLCL-Amox/PVA-VEGF scaffolds 29.2 % of VEGF is released which closely correlates with the difference in the final release between the 2 scaffold

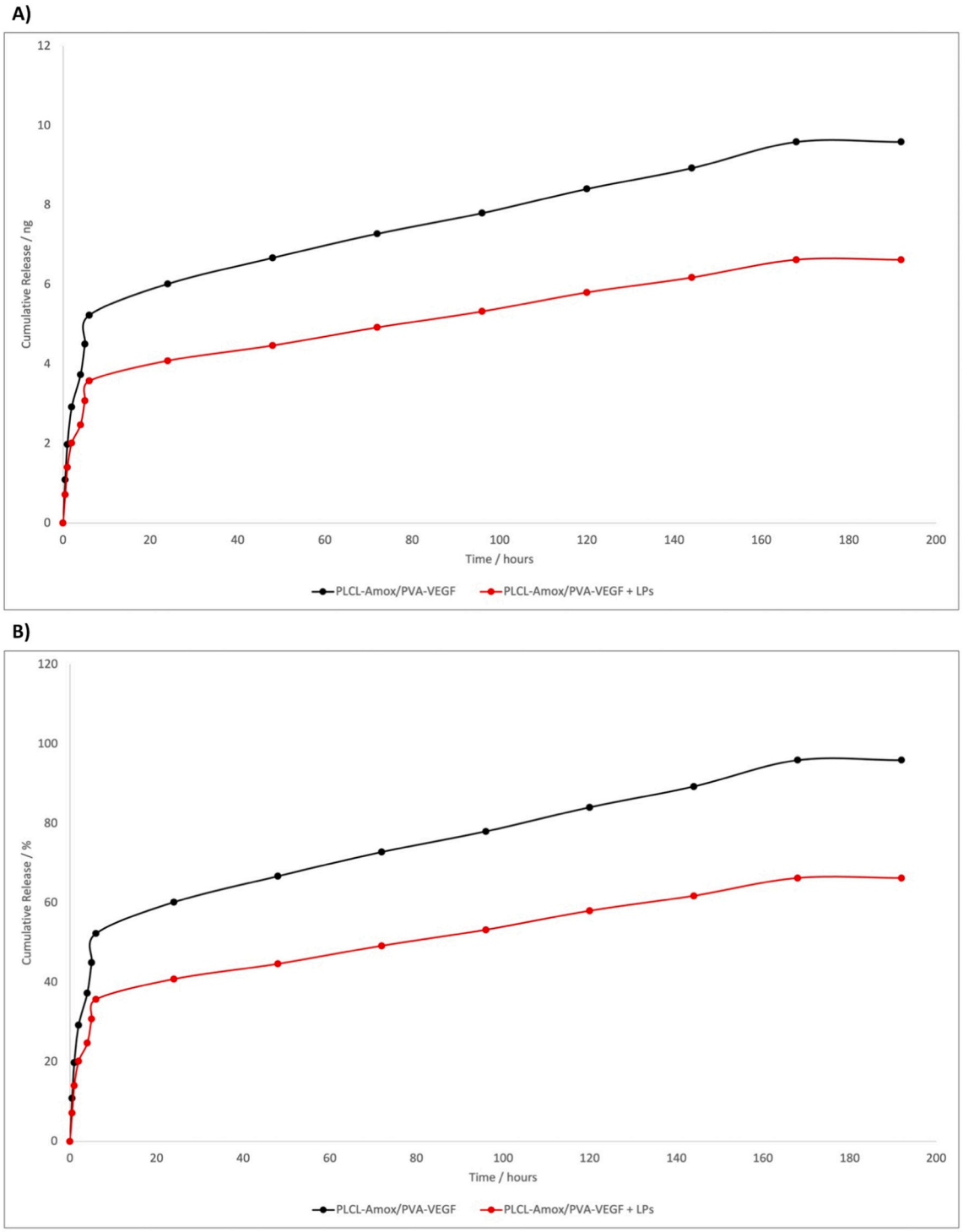

Fig. 5. Cumulative release of VEGF from the drug loaded formulations A) quantity release expressed in ng B) release expressed in % as calculated based on values of maximum Amox loading determined theoretically *via* the calculation of maximum possible VEGF loading.

groups, calculated as 29.6 %, closely matching the recorded value for VEGF release in the initial 2 h of incubation of scaffolds with no LPs adhered. The release of VEGF from both scaffold groups followed the same trend and as with the Amox release, the VEGF demonstrated a burst release within the first 6 h of incubation. VEGF release continued beyond the 7-day timepoint presented here however at these time points the quantity of VEGF detected was below the limit of detection for the ELISA kit and were therefore not included.

Problems with diabetic tissue repair and the relationship with VEGF expression have been discussed extensively [11]. Altavilla *et al.* described morphological differences and reduced breaking strength of healed wounds in diabetic mice *vs* non-diabetic controls. These changes corresponded with differences in VEGF mRNA expression and production at the wound site, with results showing that the impaired wound healing and reduced wound integrity of diabetic wounds corresponded with reductions in VEGF expression and production [53]. Given wounds in Altavilla *et al's* experiment were small compared to the chronic wounds experienced by diabetic patients, and normal levels of VEGF

production were approximately 100 pg/wound at day 6 the level of release recorded for the coaxial scaffolds produced here should be appropriate for the application. A recent study showed that VEGF may stimulate epithelialisation and collagen production with nitrous oxide, a regulator of VEGF, enhancing collagen deposition and aiding with the restoration of endothelial cell function [54]. Using this method of co-axial electrospinning to incorporate the VEGF in a core layer of water-soluble polymer mitigates the need for protective measures demonstrated previously by Tian *et al.* to ensure no damage to the protein as a result of contact with harsh solvents [55]. Previously it has been shown that electrospun water-soluble polymers demonstrate a very rapid drug release with one study showing up to 100 % of drug released within 2 h, dependent on fibre diameter [47,56]. Utilising the coaxial method of electrospinning aimed to slow the release profile from water-soluble polymers to maintain a sustained release over several days, which was successfully achieved in this study as the VEGF release from the core layer was sustained for up to 7 days *in vitro*.

3.5. Antibacterial assessment

The efficacy of the scaffolds against both Gram-positive and Gram-negative bacteria which can be found in the wound bed of diabetic foot ulcers was tested using the disc diffusion assay. Many studies have shown that the diabetic foot ulcer environment fosters a diverse range of both Gram-positive and Gram-negative species [57], *S. aureus* has been identified as the main Gram-positive strain isolated from DFU [58]. Whilst *P. mirabilis* is not the most common Gram-negative bacteria present in DFUs it has been reported to seriously worsen the infection [59]. Therefore, these species were used for investigations into the antimicrobial efficacy of scaffolds for use in DFU treatment applications.

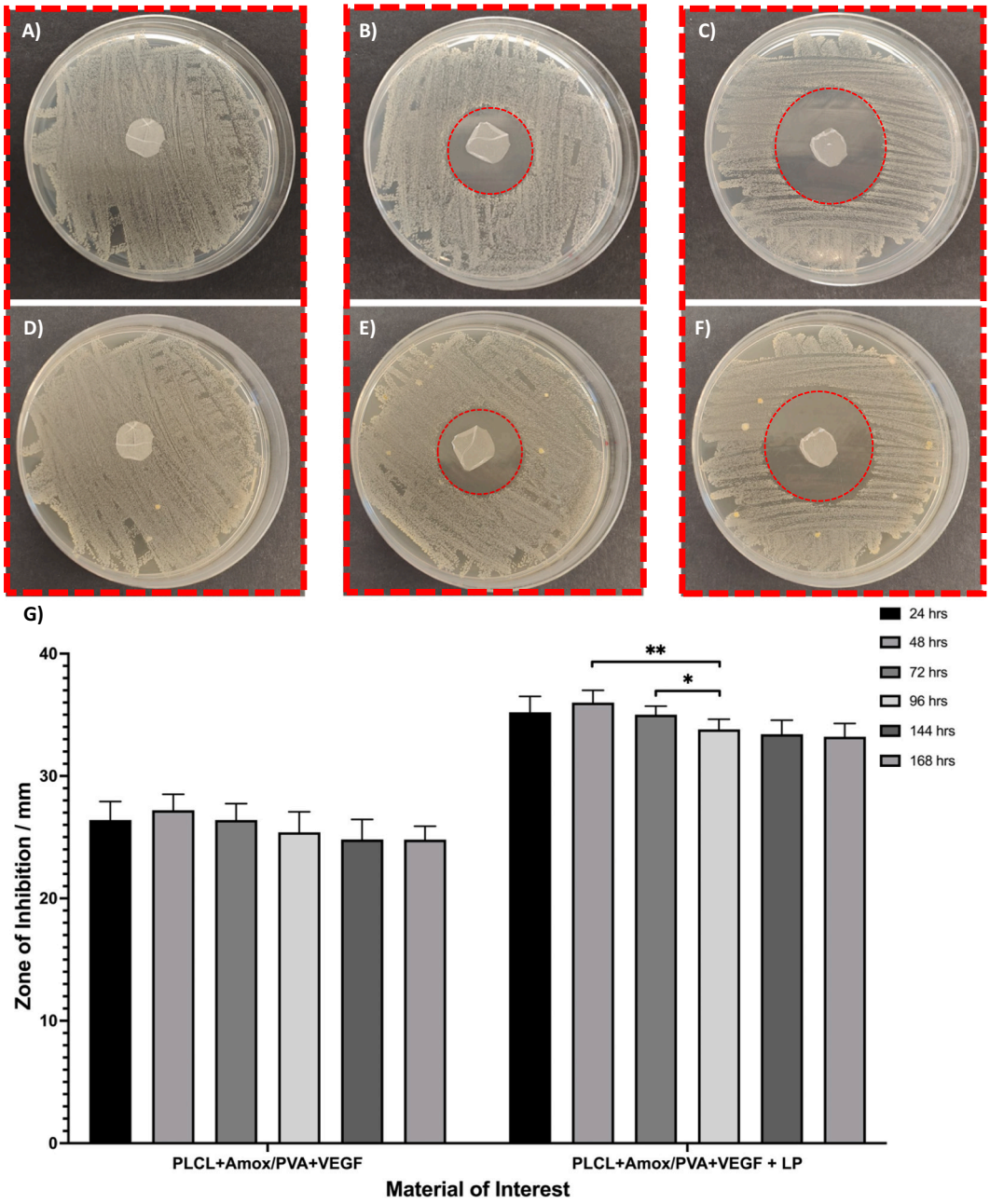

Fig. 6. Results of the disc diffusion assay using *S. aureus* as a model Gram-positive strain A–F) images showing zones of inhibition at A–C) 24 h and D–F) 7 days of incubation where A & D) show results of PLCL/PVA, B & E) show results of PLCL-Amox/PVA-VEGF and C & F) show results of scaffolds with LPs adhered G) a summary of the measured zone of inhibition diameter and statistical analysis.

After 24 h incubation of scaffolds on *S. aureus* inoculated agar, both the PLCL+Amox/PVA + VEGF and those with LPs adhered show antibacterial efficacy with clear zones observed in Fig. 6, which were not evident in the control PLCL/PVA samples. Importantly, at the 24-h time point it was evident that the delivery of the bolus dose of Amox *via* liposomal adhesion enhanced the antibacterial efficacy of the scaffolds against *S. aureus*, as demonstrated by the significant increase of the mean diameter for inhibition zone from 26.4 ± 1.5 mm, in dual-loaded scaffolds, to 35.2 ± 1.3 mm, in the samples with LPs adhered (Fig. 6C). Similar results were obtained for the study conducted using *P. mirabilis* (Fig. 7), at 24 h the zone of inhibition was significantly increased from 36.4 ± 1.1 mm to 41.6 ± 2.1 mm in samples with LPs adhered. Whilst virulence and antimicrobial resistance of *P. mirabilis* against many conventional antibacterial treatments has been attributed to the swarming growth phenomenon and flagellar motility, the drug delivery system fabricated potent antibacterial efficacy against this species [60]. Whilst it is unexpected for a β-lactam antibiotic to have increased efficacy against a Gram-negative strain, due to an extra layer of peptidoglycan rendering the cell wall more difficult for antibiotics to penetrate, the results presented in the current study show an increased efficacy towards the *P. mirabilis* [61]. However, during our previous studies, it was shown that amoxicillin, both free and encapsulated, had an increased potency against *P. mirabilis* demonstrated *via* a decreased minimum inhibitory concentration (MIC) and minimum bactericidal concentration (MBC) compared to *S. aureus* [43]. In both cases the zones of inhibition were maintained for 7 days in the *in vitro* study, highlighting the potential of these scaffolds to be used in wound dressing applications as typically dressing are changed every 5–7 days [62]. Maintenance of antibacterial efficacy for this prolonged period is attributed to the sustained release of Amox for up to 7 days, which was

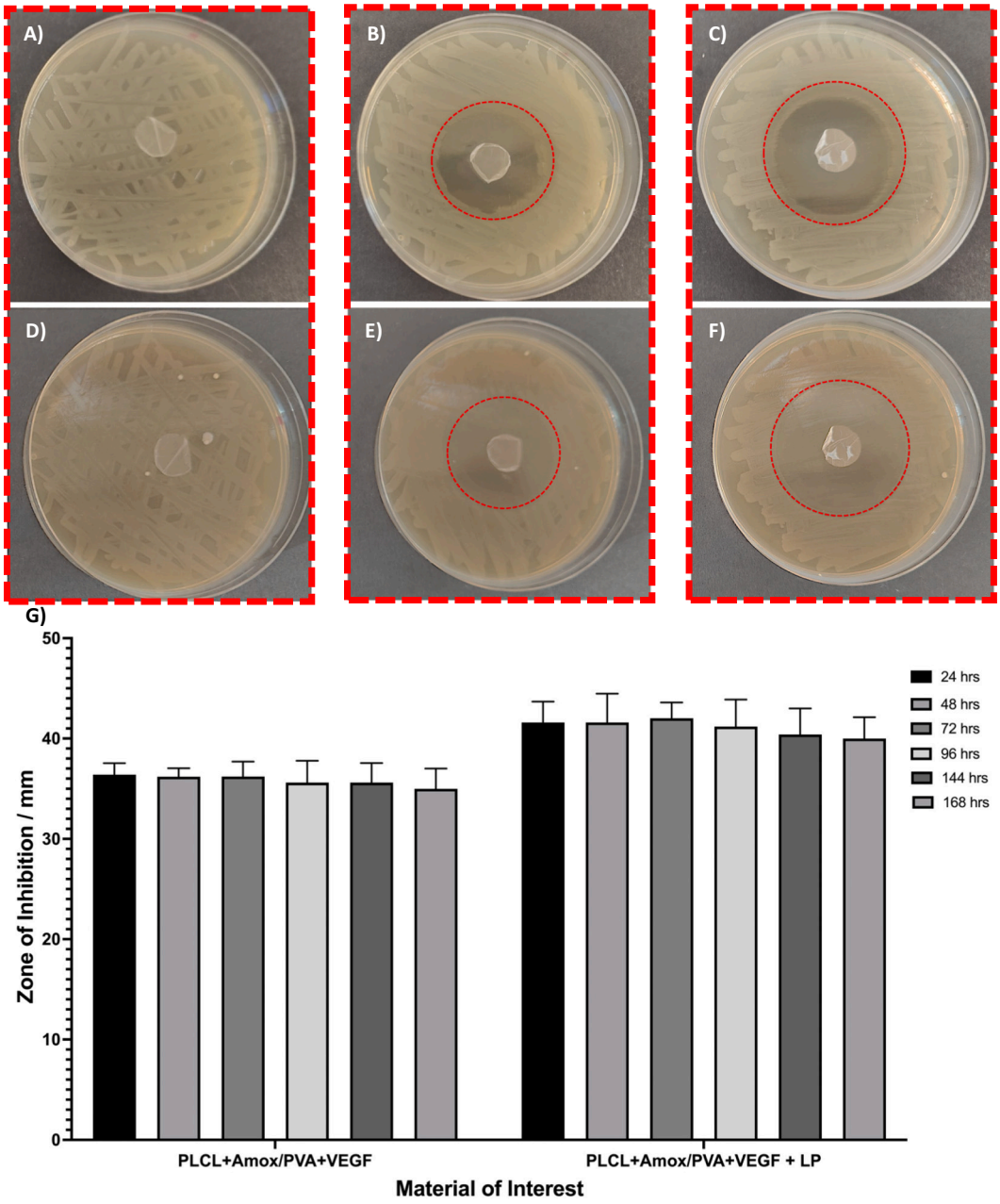

Fig. 7. Results of the disc diffusion assay using *P. mirabilis* as a model Gram-positive strain A–F) Images showing zones of inhibition at A–C) 24 h and D–F) 7 days of incubation where A & D) show results of PLCL/PVA, B & E) show results of PLCL-Amox/PVA-VEGF and C & F) show results of scaffolds with LPs adhered G) a summary of the measured zone of inhibition diameter and statistical analysis.

demonstrated previously during drug release studies (Fig. 4). The potential for antibacterial efficacy throughout the full time of wound dressing application is encouraging to ensure a reduction in bacterial colonisation at wound sites. Concerns have been previously described as to the effect organic solvents used in electrospinning processes may have on the efficacy of pharmaceutical agents [44,63]. This study proves that the Amox which was successfully incorporated into the electrospun fibres during the manufacturing process maintains its potency against both Gram-positive and Gram-negative bacteria despite exposure to such organic solvents during the manufacturing process.

3.6. Cell studies

3.6.1. Cell viability

The MTT method is a standard method of determining relative cellular metabolic activity. Viability of a primary endothelial cell line, HUVEC, was measured using the MTT assay on both the native PLCL/PVA coaxial scaffolds and the full system, PLCL+Amox/PVA + VEGF + LP. The optical densities obtained for the two scaffold groups showed a significant increase in cell viability at all time-points investigated for the dual-loaded delivery system (Fig. 8). This suggests that the VEGF release is enhancing the potential for the support of vascular cells and may improve the potential for inducing angiogenesis at wound sites during healing responses. The results here correlate with the results from the VEGF release study, the cumulative VEGF release continues to increase up to 7 days *in vitro* (Fig. 5), thus it would be expected that the HUVEC viability would continually increase in the dual-loaded scaffolds compared to the PLCL/PVA scaffolds up to 7-days *in vitro*. Importantly, the inclusion of the Amox did not possess a cytotoxic effect on the cells. Typically, cytotoxicity is described as a decrease in viability below 50 % for a given substance. It was not expected that the Amox would have any effect on the cell viability as this is a beta-lactam antibiotic which works to break down and destroy the bacterial cell wall [64]. Without the cell wall the bacteria are susceptible to osmotic and molecular pressure causing rapid cell death. This mechanism of action means that Amox demonstrates good biocompatibility due to the lack of cell wall in mammalian cells, meaning treatment with this antibiotic is unlikely to have any detrimental effect on the patients' native tissue. Additionally, if the release profiles for Amox are considered, the burst release shows the majority of Amox release within the first 5–6 h of incubation, therefore it is expected that if there is to be any cytotoxicity induced by the presence of the Amox, it would be observed within this first 6 h of release.

3.6.2. SEM cell study

An SEM cell study was completed to investigate endothelial cell attachment and proliferation on each of the scaffold groups. Fig. 9A–B shows the attachment and initial proliferation of cells cultured for 7 days on the native and dual-loaded + LP scaffolds respectively. Whilst it is evident that the PLCL/PVA scaffold supported the attachment of the HUVEC-c cells clear morphological differences can be observed between these cells and those cultured on the scaffolds containing VEGF. Cells cultured on the native scaffolds displayed a rounded morphology indicative of early attachment stages with little evidence of spreading. However, from Fig. 9B it was observed the presence of cells which were beginning to spread out across the scaffold surface with a flatter morphology and demonstrates many cells in contact with adjacent neighbouring cells. Images obtained at 7 days of culture, Fig. 9C–F, show that the drug loaded scaffolds are enabled the formation of a complete monolayer whereas in the native scaffolds results at the same time point showed that the cells were still, by enlarge, in a proliferative stage as the monolayer was incomplete with many areas of underlying fibres remaining exposed. Additionally, cell morphologies such as those highlighted in Fig. 9E displayed rounded cells raising from the monolater to facilitate mitotic activity. It was observed that across the surface of SEM images obtained for the drug loaded scaffolds at day seven, tube like structures were forming. Based on evidence presented in Fig. 9D & F it is proposed that this occurred *via* a curling of the cell monolayer to form a lumen structure such as that observed in vascular constituents.

3.6.3. Immunocytochemistry

An immunocytochemistry experiment was conducted to confirm the results of the SEM images obtained and provide additional detail on the tube-like structures which were previously observed. The immunofluorescent staining presented in Figs. 10 and 11 show that both of the scaffolds support the expression of CD31 and vWF, two key characteristic marker proteins of endothelial cells. Whilst the protein expression is observed in both sample groups there appear to be structural differences in the cell morphology between the native and drug loaded scaffolds. The CD31 expression appears diffuse throughout the cytoplasm of HUVEC cells. PLCL/PVA samples present with a cell monolayer whereas the drug loaded scaffolds show signs of vasculogenesis and angiogenesis. Figs. 10B and 11B, E and F displayed the formation of neovessels which

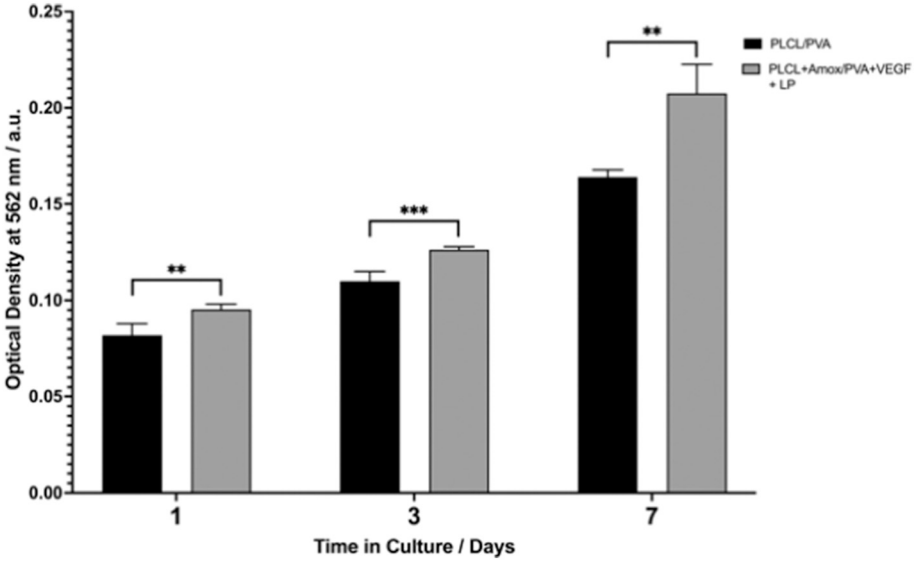

Fig. 8. Results and statistical analysis of the MTT assay investigating cell viability using HUVEC-c cells when cultured on PLCL/PVA *vs* PLCL+Amox/PVA + VEGF + LP scaffolds.

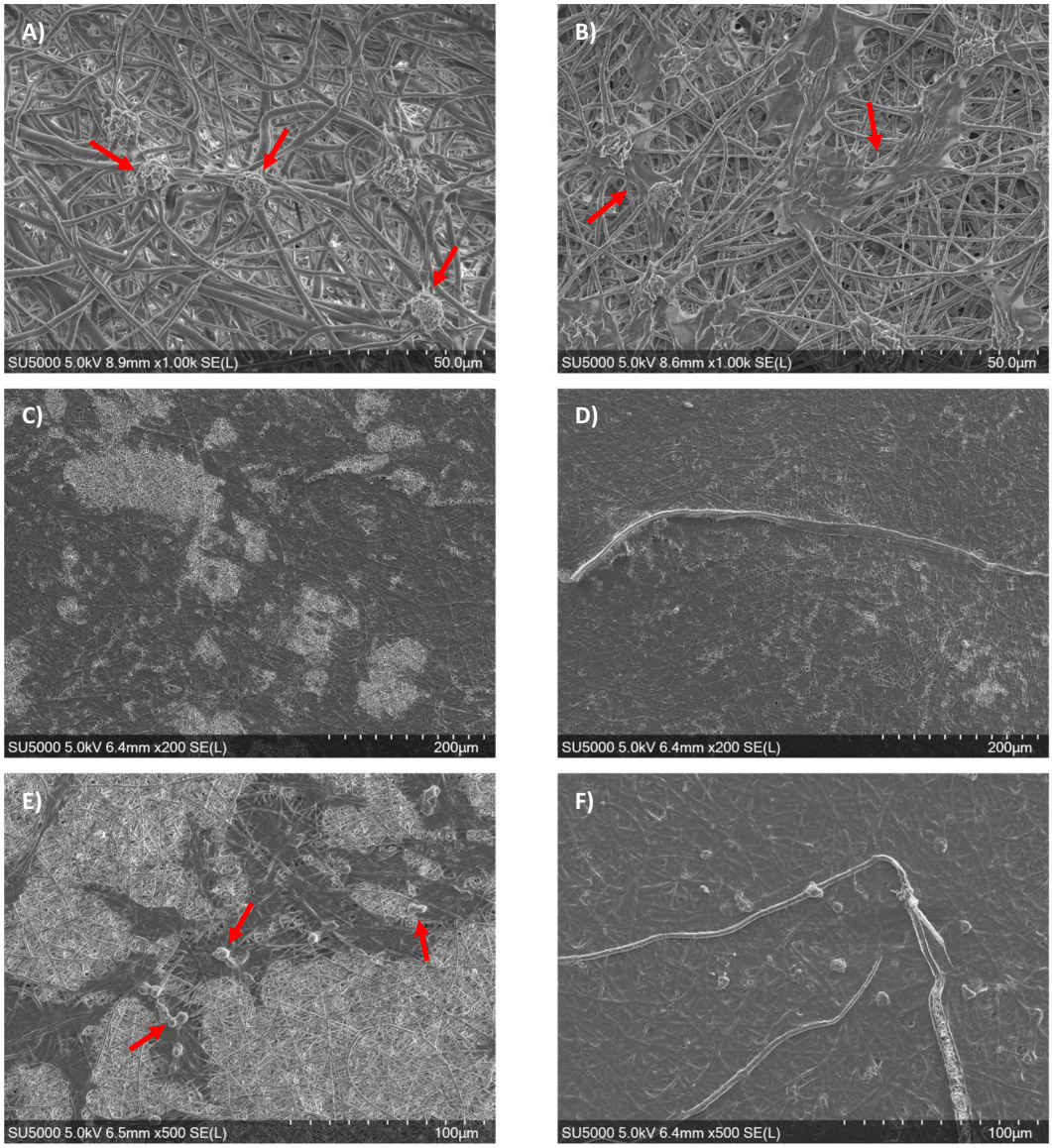

Fig. 9. SEM images showing A–B) HUVEC-c cell attachment after 6 h on A) control and B) dual-loaded + LP electrospun scaffolds C–F) HUVEC-c cell proliferation and viability after 7 days of culture on C & E) PLCL/PVA and D & F) PLCL+Amox/PVA + VEGF + LP. Red arrows in A–B demonstrate cell attachment and spreading respectively whilst those in E highlight the rounded morphology of mitotic cells. (For interpretation of the references to color in this figure legend, the reader is referred to the web version of this article.)

appear as circular structures within the cell monolayer, as highlighted by the red arrows. These neovessel like structures were also observed in the dual-loaded samples stained for vWF where the protein appears more condensed around the cell periphery than was observed in the control samples. Typically formed *via de novo* aggregation of endothelial progenitor cells these structures are required in the adaptation processes which are intrinsic to microvascular network formation and prevention of dysfunctional microcirculation [65,66]. Additionally, samples with drug loading presented with tube-like structures indicative of angiogenesis. In Fig. 10D it was observed that the HUVEC cells were involved in the formation of the tubules as nuclei were incorporated in the walls of the vessels.

The vWF-stained samples were used to analyse the tubule formation by HUVEC-c cells as shown in Fig. 12A–B. Representative images are shown to demonstrate the analysis conducted to quantify total tubule length, total branching points and total number of tubes as previously described by Kim *et al.* [65]. In agreement with the immunofluorescent imaging, results showed that the samples with VEGF incorporation provided improved *in vitro* formation of vascular constituents such as those described above. Fig. 12C–E presents the quantification of these constituent vascular elements of angiogenesis in each group, statistical analysis confirmed that there was significantly increased formation of angiogenic and vasculogenic features in samples containing VEGF. In the analysis of mean total tubule length, 328.25 µm in the control PLCL/PVA, and 2760.34 µm in the dual-loaded group confirmed that the inclusion of VEGF in the scaffold formulation significantly enhanced the potential for vasculogenic responses. Additionally, the average number of tubules was significantly increased in samples containing VEGF, however the mean tube length was not significantly changed due to the drug loading with mean lengths calculated as 97.20 and 108.40 µm in the PLCL/PVA and PLCL-Amox/PVA-VEGF + LP scaffolds respectively. These results suggest that the potential for vasculogenesis is supported by both scaffold groups with the tubules formed reaching similar lengths in both. The drug loaded scaffold however enhanced this potential presenting with more branching points and a higher number of tubules. Based on these results, it is suggested the dual-loaded scaffold may allow

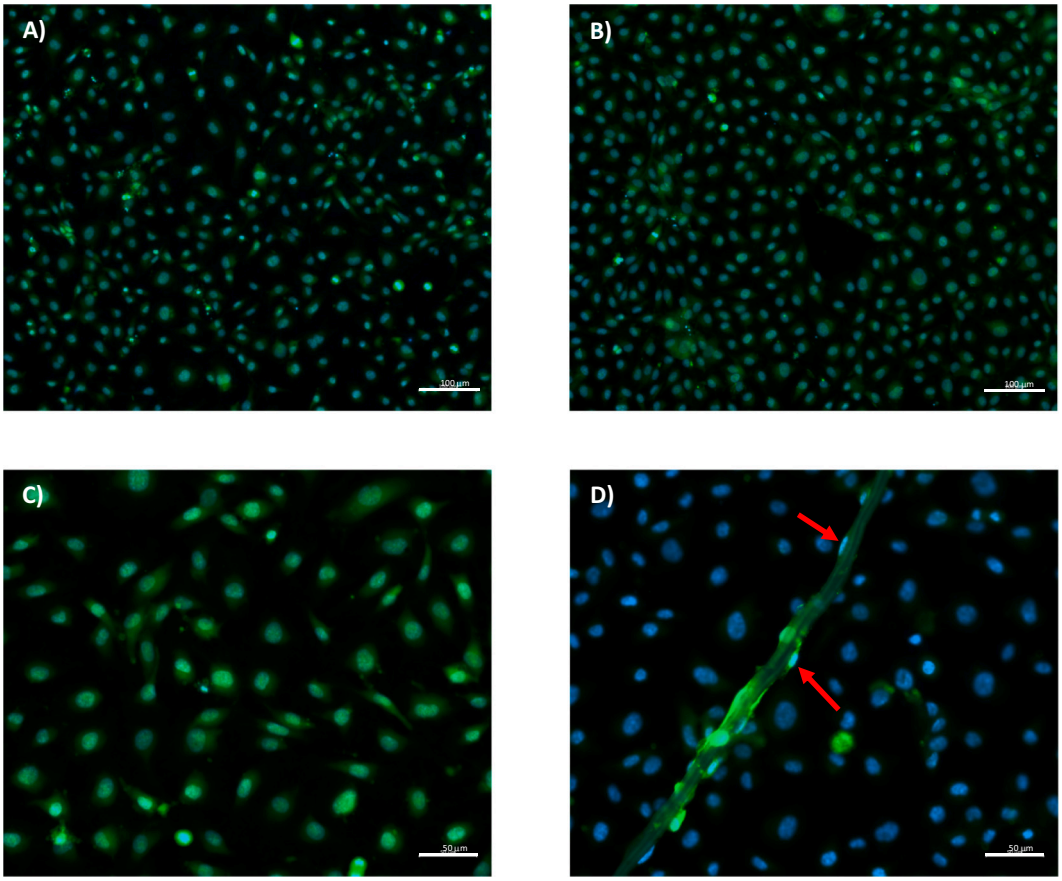

Fig. 10. Immunofluorescent images showing the expression of CD31 by primary HUVEC-c cells when cultured on the control PLCL/PVA scaffolds and PLCL+Amox/PVA + VEGF + LPs scaffolds. A & C) PLCL/PVA B & D) PLCL+Amox/PVA + VEGF + LP. Red arrows indicate vasculogenic and angiogenic features. (For interpretation of the references to color in this figure legend, the reader is referred to the web version of this article.)

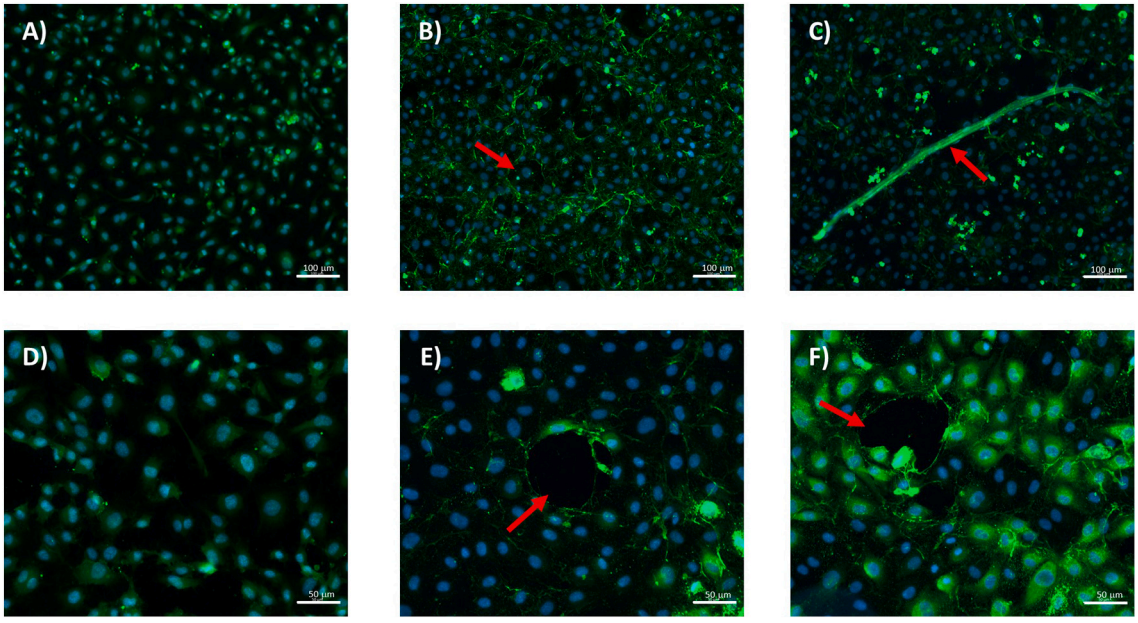

Fig. 11. Immunofluorescent images showing the expression of vWF by primary HUVEC-c cells when cultured on the control PLCL/PVA scaffolds and PLCL+Amox/PVA + VEGF + LPs scaffolds. A & D) PLCL/PVA B, C, E & F) PLCL+Amox/PVA + VEGF + LP. Red arrows indicate vasculogenic and angiogenic features. (For interpretation of the references to color in this figure legend, the reader is referred to the web version of this article.)

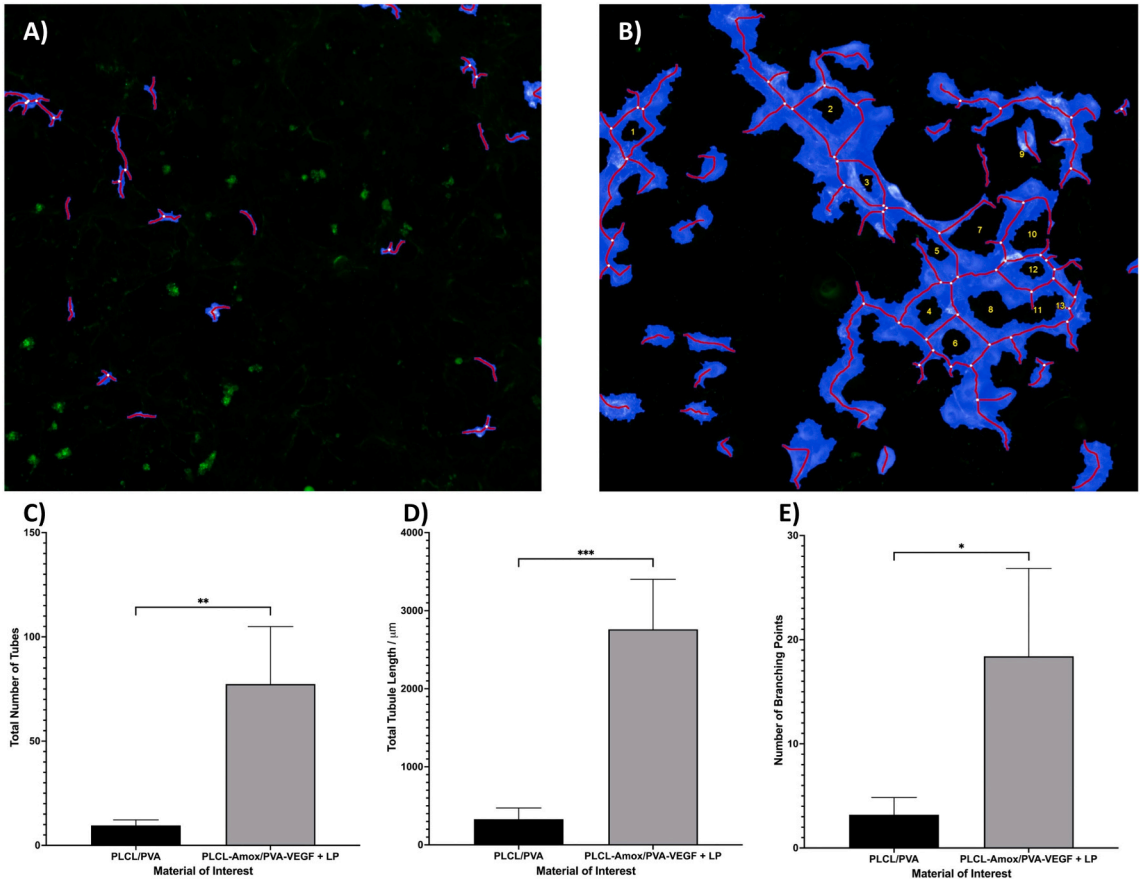

Fig. 12. Analysis of the fluorescent images to quantify vascular constituents formed by HUVEC-c cells *in vitro* on the scaffolds A–B) showing representative analytical images of A) PLCL/PVA, control scaffolds B) PLCL-Amox/PVA-VEGF+LP scaffolds C–E) quantification of mean C) total number of tubules D) total length of tubules and E) number of branching points.

a more rapid angiogenic response and vessel maturation, thereby enabling more rapid wound healing.

4. Conclusions

The work performed in this study has demonstrated the synergy between two emerging nanotherapeutic drug delivery systems: microfluidic-produced nanoparticles and electrospun nanofibers. The capacity to enhance the therapeutic efficacy of the API-loaded Electrospun fibres by adhering a loaded liposomal formulation, poses the opportunity to provide a more effective level of treatment to diabetic patients experiencing complications relating to wound healing.

Further benefits of the study propose that the use of localised delivery of Amox, such as *via* the proposed dressing could help combat the growing issue of antimicrobial resistance, due to restricting off-target activity. The capacity to simultaneously promote vascularisation and prevent infection overall reduces the healing time for diabetic wounds. From the efficacy profile displayed, the dressings could allow a weekly change of dressings for diabetic patients, instead of the daily change which can be common for many suffering from this ailment.

An additional finding of the study identified a novel sample processing method to allow the SEM imaging of adhered liposomes without the requirement for cryo-SEM.

The dressings have shown to possess antimicrobial and angiogenic activity *in vitro*, however, further characterisation *via* differential scanning calorimetry (DSC), or X-ray diffraction (XRD). These techniques would assist in highlighting the dressings as a more-comprehensively studied medical device. Whilst these *in vitro* studies provided encouraging results as a proof-of-concept for a novel wound dressing material, in order to confirm the potential for improved vascularisation and antibacterial efficacy, a relevant *in vivo* model should be designed.

Sources of funding

This research was funded by the Department for the Economy (DfE) through a PhD studentship.

CRediT authorship contribution statement

Robyn A. Macartney: Writing – review & editing, Writing – original draft, Validation, Methodology, Investigation, Formal analysis, Data curation, Conceptualization. **Edward Weaver:** Writing – review & editing, Writing – original draft, Validation, Methodology, Investigation, Formal analysis, Data curation. **Robyn Irwin:** Writing – review & editing, Investigation, Formal analysis, Data curation. **Matthew P. Wylie:** Writing – review & editing, Supervision, Methodology, Formal analysis. **George A. Burke:** Writing – review & editing, Supervision, Resources. **Dimitrios A. Lamprou:** Writing – review & editing, Visualization, Supervision, Resources, Project administration, Methodology, Funding acquisition, Conceptualization.

Declaration of competing interest

The authors declare that they have no known competing financial interests or personal relationships that could have appeared to influence the work reported in this paper.

Data statement

Upon request to the authors, all data for this project can be made freely available.

Appendix A. Supplementary data

Supplementary data to this article can be found online at https://doi.org/10.1016/j.bioadv.2024.213765.

References

[1] S. Patel, S. Srivastava, M.R. Singh, D. Singh, Mechanistic insight into diabetic wounds: pathogenesis, molecular targets and treatment strategies to pace wound healing, Biomed. Pharmacother. 112 (2019) (Elsevier Masson SAS).
[2] Y. Zhang, P.A. Lazzarini, S.M. McPhail, J.J. van Netten, D.G. Armstrong, R. E. Pacella, Global disability burdens of diabetes-related lower-extremity complications in 1990 and 2016, Diabetes Care 43 (5) (2020) 964–974.
[3] M. Edmonds, C. Manu, P. Vas, The current burden of diabetic foot disease, J Clin Orthop Trauma. 17 (Jun 1 2021) 88–93.
[4] S.F. Spampinato, G.I. Caruso, R. De Pasquale, M.A. Sortino, S. Merlo, The treatment of impaired wound healing in diabetes: looking among old drugs, Pharmaceuticals 13 (60) (2020).
[5] Z. Yang, R. Huang, B. Zheng, W. Guo, C. Li, W. He, et al., Highly stretchable, adhesive, biocompatible, and antibacterial hydrogel dressings for wound healing, Adv. Sci. 8 (8) (2021) 1–12.
[6] J.P.E. Junker, R.A. Kamel, E.J. Caterson, E. Eriksson, Clinical impact upon wound healing and inflammation in moist, wet, and dry environments, Adv Wound Care (New Rochelle). 2 (7) (Sep 2013) 348.
[7] S.A. Kelly, A.M. Rodgers, S.C. O'Brien, R.F. Donnelly, B.F. Gilmore, Gut check time: antibiotic delivery strategies to reduce antimicrobial resistance, Trends Biotechnol. 38 (4) (2020) 447–462.
[8] M. Malone, T. Bjarnsholt, A.J. McBain, G.A. James, P. Stoodley, D. Leaper, et al., The prevalence of biofilms in chronic wounds: a systematic review and meta-analysis of published data, J. Wound Care 26 (1) (2017) 20–25.
[9] U. Trivedi, S. Parameswaran, A. Armstrong, D. Burgueno-Vega, J. Griswold, S. Dissanaike, et al., Prevalence of multiple antibiotic resistant infections in diabetic versus nondiabetic wounds, J Pathog. (2014) 173053 (1–6).
[10] G. Boschetti, D. Sgarabotto, M. Meloni, M. Bruseghin, C. Whisstock, M. Marin, et al., Antimicrobial resistance patterns in diabetic foot infections, an epidemiological study in northeastern Italy, Antibiotics 10 (10) (Oct 1 2021).
[11] G. Niu, X. Chen, Vascular endothelial growth factor as an anti-angiogenic target for cancer therapy, Curr. Drug Targets 11 (8) (Jun 27 2010) 1000.
[12] K.E. Johnson, T.A. Wilgus, Vascular endothelial growth factor and angiogenesis in the regulation of cutaneous wound repair, Adv Wound Care (New Rochelle). 3 (10) (Oct 10 2014) 647.
[13] S. Chen, B. Liu, M.A. Carlson, A.F. Gombart, D.A. Reilly, J. Xie, Recent advances in electrospun nanofibers for wound healing, Nanomedicine 12 (11) (Jun 1 2017) 1335–1352.
[14] W. Song, X. Yu, D.C. Markel, T. Shi, W. Ren, Coaxial PCL/PVA electrospun nanofibers: osseointegration enhancer and controlled drug release device, Biofabrication 5 (3) (2013).
[15] R. Chen, C. Huang, Q. Ke, C. He, H. Wang, X. Mo, Preparation and characterization of coaxial electrospun thermoplastic polyurethane/collagen compound nanofibers for tissue engineering applications, Colloids Surf. B: Biointerfaces 79 (2) (2010) 315–325.
[16] B. Chatin, M. Mével, J. Devallière, L. Dallet, T. Haudebourg, P. Peuziat, et al., Liposome-based formulation for intracellular delivery of functional proteins, Mol Ther Nucleic Acids. (2015) 4.
[17] P.K. Ghosh, Liposome-assisted delivery of enzymes and proteins, Liposomal Encapsulation in Food Science and Technology. (2023) 87–111.
[18] A. Gonzalez Gomez, Z. Hosseinidoust, Liposomes for antibiotic encapsulation and delivery, ACS Infect Dis. 6 (5) (2020) 896–908.
[19] M. Li, C. Du, N. Guo, Y. Teng, X. Meng, H. Sun, et al., Composition design and medical application of liposomes, Eur. J. Med. Chem. 164 (2019) 640–653.
[20] D. Dehnad, B. Emadzadeh, B. Ghorani, G. Rajabzadeh, N. Tucker, S.M. Jafari, Bioactive-loaded nanovesicles embedded within electrospun plant protein nanofibers; a double encapsulation technique, Food Hydrocoll. 141 (2023) (Elsevier B.V.).
[21] N. Monteiro, M. Martins, A. Martins, N.A. Fonseca, J.N. Moreira, R.L. Reis, et al., Antibacterial activity of chitosan nanofiber meshes with liposomes immobilized releasing gentamicin, Acta Biomater. 18 (May 1 2015) 196–205.
[22] J. Chen, H. Pan, H. Duan, W. Deng, F. Zhang, X. Yang, et al., Self-assembled liposome from core-sheath chitosan-based fibres for buccal delivery of carvedilol: formulation, characterization and in vitro and ex vivo buccal absorption, J. Pharm. Pharmacol. 72 (3) (Mar 1 2020) 343–355.
[23] A. Mickova, M. Buzgo, O. Benada, M. Rampichova, Z. Fisar, E. Filova, et al., Core/shell nanofibers with embedded liposomes as a drug delivery system, Biomacromolecules 13 (4) (Apr 2012) 952–962.
[24] S. Antimisiaris, A novel design of PVA electrospun nanofibrous scaffold incorporating liposomes as drug delivery carriers for tissue engineering, Annals of Biomedical Technology & Engineering. (2018) 1.
[25] C. Zylberberg, S. Matosevic, Bioengineered liposome-scaffold composites as therapeutic delivery systems, Ther. Deliv. 8 (6) (Jun 1 2017) 425–445.
[26] B.K. Tarus, N. Fadel, A. Al-Oufy, M. El-Messiry, Investigation of mechanical properties of electrospun poly (vinyl chloride) polymer nanoengineered composite, J Eng Fiber Fabr. (2020) 15.
[27] A. Staffa, K. Vocetkova, V. Sovkova, M. Rampichova, E. Filova, E. Amler, Polycaprolactone nanofiber mesh with adhered liposomes as a simple delivery system for bioactive growth factors, Translational Medicine Reports. 1 (6716) (2017) 58–63.
[28] N. Monteiro, A. Martins, R. Pires, S. Faria, N.A. Fonseca, J.N. Moreira, et al., Immobilization of bioactive factor-loaded liposomes on the surface of electrospun nanofibers targeting tissue engineering, Biomater. Sci. 2 (2014) 1195–1209.
[29] F. Sommonte, E. Weaver, E. Mathew, N. Denora, D.A. Lamprou, In-house innovative "diamond shaped" 3D printed microfluidic devices for lysozyme-loaded liposomes, Pharmaceutics 14 (11) (2022).
[30] M.P. Wylie, S.E.J. Bell, P. Nockemann, R. Bell, C.P. McCoy, Phosphonium ionic liquid-infused poly(vinyl chloride) surfaces possessing potent antifouling properties, ACS Omega 5 (14) (Apr 14 2020) 7771–7781.
[31] K. Czamara, K. Majzner, M.Z. Pacia, K. Kochan, A. Kaczor, M. Baranska, Raman spectroscopy of lipids: a review, J. Raman Spectrosc. 46 (1) (2015) 4–20.
[32] L. Wang, G. Zhou, Guan X li, Zhao L. Rapid preparation of surface-enhanced Raman substrate in microfluidic channel for trace detection of amoxicillin. Spectrochim Acta A Mol Biomol Spectrosc. 5 (2020 Jul) 235.
[33] F.K. Metze, S. Sant, Z. Meng, H.A. Klok, K. Kaur, Swelling-activated, soft mechanochemistry in polymer materials, Langmuir 39 (2023) 3546–3557.
[34] L.A. Setton, H. Tohyama, V.C. Mow, Swelling and curling behaviors of articular cartilage, J. Biomech. Eng. 120 (1998) 355–361.
[35] E. Reyssat, L. Mahadevan, Hygromorphs: from pine cones to biomimetic bilayers, J. R. Soc. Interface 6 (2009) 951–957.
[36] J. Dervaux, Amar M. Ben, Mechanical instabilities of gels, Annu Rev Condens Matter Phys. 3 (2012) 311–332.
[37] F. Elhaouzi, A. Mdarhri, C. Brosseau, I. El Aboudi, A. Almaggoussi, Effects of swelling on the effective mechanical and electrical properties of a carbon black-filled polymer, Polym. Bull. 76 (2019) 2765–2776.
[38] A. Kalra, A. Lowe, A.J. Am, Mechanical behaviour of skin: a review, J. Mater. Sci. Eng. 5 (2016) 4.
[39] M. Pawlaczyk, M. Lelonkiewicz, M. Wieczorowski, Age-dependent biomechanical properties of the skin, Advances in Dermatology and Allergology/Postępy Dermatologii i Alergologii. 30 (5) (2013) 302.
[40] M.F. Griffin, B.C. Leung, Y. Premakumar, M. Szarko, P.E. Butler, Comparison of the mechanical properties of different skin sites for auricular and nasal reconstruction. Journal of, Otolaryngol. Head Neck Surg. 46 (1) (Apr 18 2017).
[41] A.J. Gallagher, A.N. Anniadh, K. Bruyere, M. Otténio, H. Xie, M.D. Gilchrist, Dynamic Tensile Properties of Human Skin, International Research Council on Biomechanics of Injury, 2012, pp. 494–502.
[42] C. Flynn, A. Taberner, P. Nielsen, Modeling the mechanical response of in vivo human skin under a rich set of deformations, Ann. Biomed. Eng. 39 (7) (Jul 11 2011) 1935–1946.
[43] A. Ní Annaidh, K. Bruyère, M. Destrade, M.D. Gilchrist, M. Otténio, Characterization of the anisotropic mechanical properties of excised human skin, J. Mech. Behav. Biomed. Mater. 5 (1) (2012) 139–148.
[44] Y. Ding, W. Li, F. Zhang, Z. Liu, N. Zanjanizadeh Ezazi, D. Liu, et al., Electrospun fibrous architectures for drug delivery, tissue engineering and cancer therapy, Adv. Funct. Mater. 29 (2) (Jan 10 2019).
[45] J. Wu, Z. Zhang, J. Gu, W. Zhou, X. Liang, G. Zhou, et al., Mechanism of a long-term controlled drug release system based on simple blended electrospun fibers, J. Control. Release 320 (2020) 337–346.
[46] H. Peng, S. Zhou, T. Guo, Y. Li, X. Li, J. Wang, et al., In vitro degradation and release profiles for electrospun polymeric fibers containing paracetanol, Colloids Surf. B: Biointerfaces 66 (2008) 206–212.
[47] W. Cui, X. Li, X. Zhu, G. Yu, S. Zhou, J. Weng, Investigation of drug release and matrix degradation of electrospun poly(DL-lactide) fibers with paracetanol inoculation, Biomacromolecules 7 (5) (2006) 1623–1629.
[48] P.L. Ritger, N.A. Peppas, A simple equation for description of solute release I. Fickian and non-fickian release from non-swellable devices in the form of slabs, spheres, cylinders or discs, J. Control. Release 5 (1) (1987) 23–36.
[49] M.V. Natu, H.C. de Sousa, M.H. Gil, Effects of drug solubility, state and loading on controlled release in bicomponent electrospun fibers, Int. J. Pharm. 397 (2010) 50–58.
[50] Y. Sun, S. Cheng, W. Lu, Y. Wang, P. Zhang, Q. Yao, Electrospun fibers and their application in drug controlled release, biological dressings, tissue repair, and enzyme immobilization, RSC Adv. 9 (44) (2019) 25712–25729.
[51] D. Altavilla, A. Saitta, D. Cucinotta, M. Galeano, B. Deodato, M. Colonna, et al., Inhibition of lipid peroxidation restores impaired vascular endothelial growth factor expression and stimulates wound healing and angiogenesis in the genetically diabetic mouse, Diabetes 50 (3) (2001) 667–674.
[52] H. Entero, VEGF enhances angiogenic response in experimental wounds as measured by tensile properties of the wound, increased epithelialization, and decreased time to closure, Ostomy Wound Manage 53 (4) (2007) 94–95.
[53] L. Tian, M.P. Prabhakaran, X. Ding, D. Kai, S. Ramakrishna, Emulsion electrospun vascular endothelial growth factor encapsulated poly(l-lactic acid-co-ε-caprolactone) nanofibers for sustained release in cardiac tissue engineering, J. Mater. Sci. 47 (7) (2012) 3272–3281.
[54] P. Taepaiboon, U. Rungsardthong, P. Supaphol, Drug-loaded electrospun mats of poly(vinyl alcohol) fibres and their release characteristics of four model drugs, Nanotechnology 17 (9) (2006) 2317–2329.

[55] P. Shanmugam, M. Jeya, S.S. Linda, The bacteriology of diabetic foot ulcers, with a special reference to multidrug resistant strains, J. Clin. Diagn. Res. 7 (3) (2013) 441–445.
[56] J. Lee, M. Mashayamombe, T.P. Walsh, B.K.P. Kuang, G.N. Pena, S. Vreugde, et al., The bacteriology of diabetic foot ulcers and infections and incidence of Staphylococcus aureus Small Colony Variants, J. Med. Microbiol. 72 (6) (2023).
[57] A.N. Khayyat, H.A. Abbas, M.F.A. Mohamed, H.Z. Asfour, M.T. Khayat, T. S. Ibrahim, et al., Not only antimicrobial: metronidazole mitigates the virulence of proteus mirabilis isolated from macerated diabetic foot ulcer, Applied Sciences (Switzerland). 11 (15) (2021).
[58] A. Filipiak, M. Chrapek, E. Literacka, M. Wawszczak, S. Głuszek, M. Majchrzak, et al., Pathogenic factors correlate with antimicrobial resistance among clinical Proteus mirabilis strains, Front. Microbiol. (2020) 11.
[59] J. Davis, Chapter 2 - pharmacologic principles, in: Equine Internal Medicine, 4th ed., Elsevier Health Sciences, 2018, pp. 79–137.
[60] J.F. Guest, G.W. Fuller, P. Vowden, Diabetic foot ulcer management in clinical practice in the UK: costs and outcomes, Int. Wound J. 15 (1) (2018) 43–52.
[61] K. Grodowska, A. Parczewski, Organic solvents in the pharmaceutical industry, Polish Pharmaceutical Society. 67 (1) (2010) 3–12.
[62] S. Alfei, A.M. Schito, β-Lactam antibiotics and β-lactamase enzymes inhibitors, part 2: our limited resources, Pharmaceuticals 15 (4) (Apr 1 2022).
[63] S. Negri, P. Faris, R. Berra-Romani, G. Guerra, F. Moccia, Endothelial transient receptor potential channels and vascular remodeling: extracellular Ca2 + entry for angiogenesis, arteriogenesis and vasculogenesis. Front Physiol. 10 (Jan 21 2020).
[64] A.J. Leblanc, L. Krishnan, C.J. Sullivan, S.K. Williams, J.B. Hoying, Microvascular repair: post-angiogenesis vascular dynamics, Microcirculation 19 (8) (2012) 676–695.
[65] T.H. Kim, Y. Jung, S.H. Kim, Nanofibrous electrospun heart decellularized extracellular matrix-based hybrid scaffold as wound dressing for reducing scarring in wound healing, Tissue Eng. Part A 24 (9–10) (2018) 830–848.